

Space borne tropospheric nitrogen dioxide (NO₂) observations from 2005-2020 over the Yangtze River Delta (YRD), China: variabilities, implications, and drivers

Hao Yin^{1, 2, #}, Youwen Sun^{1, #, †}, Justus Notholt³, Mathias Palm³, and Cheng Liu^{2, 4, 5, 6, †}

¹Key Laboratory of Environmental Optics and Technology, Anhui Institute of Optics and Fine Mechanics, HFIPS, Chinese Academy of Sciences, Hefei 230031, China

²Department of Precision Machinery and Precision Instrumentation, University of Science and Technology of China, Hefei 230026, China

³University of Bremen, Institute of Environmental Physics, P. O. Box 330440, 28334 Bremen, Germany

⁴Anhui Province Key Laboratory of Polar Environment and Global Change, University of Science and Technology of China, Hefei 230026, China

⁵Center for Excellence in Regional Atmospheric Environment, Institute of Urban Environment, Chinese Academy of Sciences, Xiamen 361021, China

⁶Key Laboratory of Precision Scientific Instrumentation of Anhui Higher Education Institutes, University of Science and Technology of China, Hefei 230026, China

[#]These authors contributed equally to this work

[†]Correspondence to: Youwen Sun (ywsun@aiofm.ac.cn) and Cheng Liu (chliu81@ustc.edu.cn)

Abstract

Nitrogen dioxide (NO₂) is mainly affected by local emission and meteorology rather than long-range transport. Accurate knowledge of its long-term variabilities and drivers are significant for understanding the evolutions of economic and social development, anthropogenic emission, and the effectiveness of pollution control measures on regional scale. In this study, we quantify the long-term variabilities and the underlying drivers of NO₂ from 2005 to 2020 over the Yangtze River Delta (YRD), one of the most densely populated and highly industrialized city clusters in China, using OMI space borne observations and the multiple linear regression (MLR) model. We have compared the space borne tropospheric results to the surface in-situ data, yielding correlation coefficients of 0.8 to 0.9 over all megacities within the YRD. As a result, the tropospheric NO₂ column measurements can be used as representatives of near-surface conditions, and we thus only use ground-level meteorological data for MLR regression. The inter-annual variabilities of tropospheric NO₂ vertical column densities (NO₂ VCD_{trop}) from 2005 to 2020 over the YRD can be divided into two stages. The first stage was from 2005 to 2011, which showed overall increasing trends with a wide range of (1.91 ± 1.50) to $(6.70 \pm 0.10) \times 10^{14}$ molecules/cm²·yr⁻¹ ($p < 0.01$) over the YRD. The second stage was from 2011 to 2020, which showed over all decreasing trends of (-6.31 ± 0.71) to $(-11.01 \pm 0.90) \times 10^{14}$ molecules/cm²·yr⁻¹ ($p < 0.01$) over each of the megacities. The seasonal cycles of NO₂ VCD_{trop} over the YRD are mainly driven by meteorology (81.01% - 83.91%) except during winter when anthropogenic emission contributions are pronounced (16.09% - 18.99%). The inter-annual variabilities of NO₂ VCD_{trop} are mainly driven by anthropogenic emission (69.18% - 81.34%) except for a few years such as 2018 which are partly attributed to meteorology anomalies (39.07% - 91.51%). The increasing trends in NO₂ VCD_{trop} from 2005 to 2011 over the YRD are mainly attributed to high energy consumption associated with rapid economic growth which causes

significant increases in anthropogenic NO₂ [emission](#). The decreasing trends in [NO₂ VCD_{trop}](#) from 2011 to 2020 over the YRD are mainly attributed to the stringent clean air measures which either adjust high energy industrial structure toward low energy industrial structure or directly reduce pollutant emissions from different industrial sectors.

Keywords: OMI; nitrogen dioxide; Emissions; Meteorology; Multiple linear regression model

1. Introduction

As a major tropospheric pollutant, nitrogen dioxide (NO₂) not only threatens human health and crop growth but also involves in a series of atmospheric photochemical reactions (Yin et al., 2019; Wang et al., 2011; Geddes et al., 2012). NO₂ is a crucial precursor in the formation of ozone (O₃), particulate matter (PM), acid rain, and photochemical smog in the troposphere (Yin et al., 2021a; Lu et al., 2019a; Lu et al., 2019b; Sun et al., 2018). Since severe NO₂ pollution increases the risk of respiratory disease and is highly associated with mortality (Meng et al., 2021; MacIntyre et al., 2014; Tao et al., 2012), many countries take the NO₂ level as an important pollution indicator of air quality (Xue et al., 2020). The sources of tropospheric NO₂ are mainly from anthropogenic [emission](#) through high temperature combustions, like transportation (vehicles, ships, and airplanes) and industrial facilities (petrochemicals and power plants) (Zheng et al., 2018b; Chi et al., 2021; van Geffen et al., 2015). Additional minor sources of NO₂ are attributed to natural emissions from [the biogeochemical reactions](#) in soil, volcanic eruption, and lightning (Bond et al., 2001; Zhang et al., 2003; Lu et al., 2021). The dominant sink of tropospheric NO₂ is attributed to a chemical destruction which first converts NO₂ into nitric acid (HNO₃) and peroxyacetyl nitrate (PAN) which then are by dry or wet deposition (Browne et al., 2013). Due to a short lifetime of a few hours, tropospheric NO₂ is heavily affected by local [emission](#) and meteorology rather than long-range transport (Kim et al., 2015; Cheng et al., 2012).

Many scientists have used a suite of active and passive observation technologies onboard ground-based, vehicle-based, ship-based, airborne, or space borne platforms to assess the temporal-spatial variabilities of NO₂ and identify their driving forces in different regions around the globe (Richter et al., 2005; Jiang et al., 2018; Liu et al., 2018; Zhang et al., 2021; Schreier et al., 2015; Shaiganfar et al., 2017). Among all observation technologies and platforms, space borne remote sensing observations have their unique features. By validating with ground-based remote sensing or balloon observations, space borne observations can provide global NO₂ dataset with a reasonable accuracy. Typical space borne instruments include the SCIAMACHY, GOME, OMI, and TROPOMI, which have been widely used in scientific investigations of global nitrogen cycle, O₃ formation regime, and regional pollution & transport, quantification of NO₂ emissions from biomass burning regions, megacities, and industrial facilities, and validation of shipborne observations and atmospheric chemical transport models (CTMs) (Richter et al., 2005; Bechle et al., 2013; Boersma et al., 2011; Ghude et al., 2009; Lamsal et al., 2008). Using space borne observations to derive long term trends of NO₂ and their drivers not only provides valuable information for evaluation of regional [emissions](#), but also improves our understanding of atmospheric evolutions. (Richter et al., 2005) first investigated the inter annual variabilities of tropospheric NO₂ vertical column densities ([NO₂ VCD_{trop}](#)) from space with GOME and SCIAMACHY observations during 1996-2004. (Richter et al., 2005) found substantial reductions in NO₂ VCDs over some areas of Europe and the USA, but a highly significant increase of about 50%—with an accelerating trend in annual growth rate—

over the industrial areas of China. In a subsequent study, (Ghude et al., 2009) found the same phenomenon as those of (Richter et al., 2005) with GOME and SCIAMACHY observations from 1996 to 2006, which disclosed that $\text{NO}_2 \text{ VCD}_{\text{trop}}$ showed increasing trends over the rapidly developing regions (China: $11 \pm 2.6\%/ \text{year}$, South Asia: $1.76 \pm 1.1\%/ \text{year}$, Middle East Africa: $2.3 \pm 1 \%/ \text{year}$) and decreasing or level-off trends over the developed regions (US: $-2 \pm 1.5\%/ \text{year}$, Europe: $0.9 \pm 2.1\%/ \text{year}$). With multiple satellite platforms including GOME, SCIAMACHY, OMI, and GOME-2, (Hilboll et al., 2013) also found 5% to 10% yr^{-1} of increasing trends for $\text{NO}_2 \text{ VCD}_{\text{trop}}$ over eastern Asia during 1996 to 2011. With the OMI observations, (Lamsal et al., 2015) have quantified the NO_2 trend from 2005 to 2013 over the US and (Krotkov et al., 2016) have investigated the NO_2 trends over different countries for the period of 2005–2014.

Along with the great advances in social and economic development in recent decades, air quality in China has changed dramatically (Sun et al., 2020; Sun et al., 2021c; Yin et al., 2020; Yin et al., 2021c; Yin et al., 2021d). China has implemented a series of clean air measures in different stages to tackle air pollution across China. One of the landmark clean air measures could be the Action Plan on the Prevention and Control of Air Pollution implemented in 2013, which launched many stringent measures to improve air quality across China. These measures include the reduction of air pollutant emissions, the adjustment of industrial structure and energy mix, the establishment of early-warning systems and monitoring for air pollution, and other compulsive policies (China State Council, 2013). Both space borne and ground-based observations have witnessed the effectiveness of these successful policies. The OMI $\text{NO}_2 \text{ VCD}_{\text{trop}}$ have been decreased by 21% from 2011 to 2015 over 48 cities of China (Liu et al., 2017). The national averaged surface NO_2 recorded by the China National Environmental Monitoring Center (CNEMC) network has significantly decreased from $(16.68 \pm 4.82) \text{ ppbv}$ in 2013 to $(11.29 \pm 3.25) \text{ ppbv}$ in 2020 (Lin et al., 2021).

In this study, we use $\text{NO}_2 \text{ VCD}_{\text{trop}}$ from 2005–2020 provided by OMI to comprehensively evaluate the long-term trends, implications, and underlying drivers of NO_2 over the Yangtze River Delta (YRD, including Anhui, Jiangsu, Shanghai, and Zhejiang Provinces, Table S1). In addition to anthropogenic emission, meteorology also drives NO_2 variability by affecting emissions, transport, chemical production, and scavenging. The relationships of NO_2 against meteorological variables are complex and are region and time dependent. In present work, we separate the contributions of meteorology and anthropogenic emission to the NO_2 variability by multiple linear regression (MLR) model over the major cities (Hefei, Nanjing, Suzhou, Shanghai, Hangzhou, Ningbo) within the YRD. As one of the three most densely populated and highly industrialized city clusters in China, the YRD has long been identified as a key region for air pollution mitigation. This study can not only improve our understanding of temporal spatial NO_2 evolutions in the atmosphere but also provides valuable information for future clean air policy. We introduce detailed descriptions of OMI and ground-level NO_2 products in section 2.1, and meteorological fields in section 2.2. The method for separating contributions of meteorology and anthropogenic emission is presented in section 2.3. Sections 3.1 and 3.2 analyze the temporal-spatial variabilities of tropospheric NO_2 from 2005 to 2020 over the YRD on provincial and megacity levels, respectively. A comparison between the OMI NO_2 product and the ground-level measurements is performed in section 3.3. We discuss the implications and underlying drivers of the variabilities of tropospheric NO_2 from 2005 to 2020 over the YRD in section 4. We conclude this study in section 5.

2. Data and method

2.1 Observation data

2.1.1 OMI NO₂ product

OMI is a hyperspectral atmospheric composition detection instrument onboard the National Aeronautics and Space Administration (NASA) Aura Earth Observing System (EOS) satellite launched in July, 2004 (Boersma et al., 2007). The EOS satellite flies over a low-Earth orbit at an altitude of about 710 km. The local overpass time (LT) of OMI satellite is about 13:30 in early afternoon. The retrieval micro window for NO₂ VCDs lies in between 405 nm and 465 nm with a spectral resolution of about 0.5nm (Marchenko et al., 2015). The spatial resolution of OMI measurements is 13 × 24 km² at nadir. OMI provides observations of O₃, NO₂, SO₂, aerosol, cloud, HCHO, BrO, and OCIO with nearly daily global coverage (Levelt et al., 2006). The daily LV3 data product of NO₂ VCD_{trop} data (GES DISC; <http://disc.sci.gsfc.nasa.gov>, last accessed: 1 September 2021) which is a gridded data with a 0.25° × 0.25° spatial resolution are used in this study. The NO₂ VCD_{trop} are calculated by Stratosphere–troposphere separation (STS) scheme proposed by numerous previous studies (Bucsela et al., 2013; Lamsal et al., 2014; Goldberg et al., 2017). The STS scheme first subtract the stratospheric NO₂ slant column densities (SCDs) from the total NO₂ SCDs and then it divides the resulting tropospheric NO₂ SCDs by the tropospheric air mass factor (AMF). The formulation for calculating NO₂ VCD_{trop} is as follow:

$$VCD_{trop} = \frac{SCD_{total} - SCD_{strat}}{AMF_{trop}} \quad (1)$$

where AMF is defined as the ratio of the SCD to the VCD (Solomon et al., 1987),

$$AMF_{trop} = \frac{SCD_{trop}}{VCD_{trop}} \quad (2)$$

The tropospheric AMF are calculated by NO₂ profiles simulated by the Global Modeling Initiative (GMI) chemistry transport model with the horizontal resolution of 1° × 1.25° (Rotman et al., 2001). Separation of stratospheric and tropospheric columns is achieved by the local analysis of the stratospheric field over unpolluted areas (Bucsela et al., 2013). The OMI NO₂ VCD_{trop} dataset has been used in many studies to investigate O₃ formation regime and regional pollution & transport (Lin et al., 2010; Zhang et al., 2017; Duncan et al., 2013; Liu et al., 2016). In this study, only the LV3 data product collected with cloud radiance fractions of less than 30% is used (Streets et al., 2013).

2.1.2 Ground level NO₂ data

We extract ground level NO₂ data over the YRD from the China National Environmental Monitoring Center (CNEMC) network (<http://www.cnemc.cn/en/>, last access: November 26, 2021). The CNEMC network has operated more than 3000 monitoring sites that almost cover all major cities over China by 2020. The CNEMC datasets have been used in many studies for evaluation of regional atmospheric pollution & transport (Li et al., 2021; Lu et al., 2019a; Lu et al., 2020; Sun et al., 2021a; Yin et al., 2021a; Zhao et al., 2016; He et al., 2017). As one of the six key atmospheric pollutants (CO, SO₂, NO₂, PM₁₀, O₃, and PM_{2.5}) routinely measured by the CNEMC network, ground level NO₂ measurements at 188 sites in 40 cities over the YRD are available since 2014. In this study, comparisons between the OMI NO₂ data product and the ground level NO₂ measurements are only performed over 6 key megacities, i.e., Shanghai, Nanjing, Hangzhou, Suzhou, Ningbo, and Hefei, within the YRD. The population, geolocation, the number of measurement site, and data range of each city are summarized in Table 1. The number of measurement site in each city ranges

from 8 to 11, the altitude ranges from 3 to 50 m (above sea level, a.s.l.), and the population ranges from 0.9 to 2.5 million. All ground level NO₂ data at each station are measured by active differential absorption ultraviolet (UV) analyzers. We use a data quality control method following previous studies to remove unreliable NO₂ data (Lu et al., 2019a; Lu et al., 2020; Sun et al., 2021a; Yin et al., 2021a). Specifically, we first convert all hourly measurements into Z scores, we then remove the measurement if its Z score meets one of the following rules: (1) Z_i is larger or smaller than the previous value Z_{i-1} by 9 ($|Z_i - Z_{i-1}| > 9$); (2) The absolute value of Z_i is greater than 4 ($|Z_i| > 4$); (3) the ratio of the Z value to the third-order center moving average is greater than 2 ($\frac{3Z_i}{Z_{i-1}+Z_i+Z_{i+1}} > 2$), where i represents the i^{th} hourly measurement data. After removing OUTLIERS with above filter criteria, we finally average NO₂ data at all measurement sites in each city to form a city representative NO₂ dataset.

2.2 Meteorological fields

We obtain meteorological fields during 2005-2020 from the second Modern-Era Retrospective analysis for Research and Applications (MERRA-2) (Gelaro et al., 2017). This dataset is produced by the NASA Global Modeling and Assimilation Office (<https://gmao.gsfc.nasa.gov/reanalysis/MERRA-2/>, last accessed: 1 August, 2021) with a spatial resolution of $0.5^\circ \times 0.625^\circ$, temporal resolutions of 1 h for boundary layer height and surface meteorological variables, and 3 h for other variables. Previous studies have verified that meteorological fields provided by MERRA-2 match well with the meteorological parameters observed by Chinese weather stations (Song et al., 2018; Carvalho, 2019; Wang et al., 2017; Kishore Kumar et al., 2015; Zhou et al., 2017). In order to match OMI observations which are available at about 13:30 LT, the average for meteorological data is only performed between 13:00 and 14:00 LT.

2.3 Multiple linear regression (MLR) model

We establish a multiple linear regression (MLR) model to quantify the contributions of meteorology and anthropogenic **emission** to the long-term variabilities of **NO₂ VCD_{trop}** during 2005-2020 over the YRD. Similar MLR methodologies have been used in previous studies to estimate the contributions of meteorology and emission to the variabilities of O₃ and PM_{2.5} in North America, Europe and China (Li et al., 2019; Li et al., 2020; Xu et al., 2011; Zhai et al., 2019; Zhao and Wang, 2017). The meteorological parameters used in our MLR model are elaborated in Table 2.

In order to highlight the variabilities of **NO₂ VCD_{trop}**, we follow the method of previous studies and calculate **NO₂ VCD_{trop}** anomalies ($\mathbf{y}_{anomaly}$) by subtracting a reference value ($\mathbf{y}_{reference}$) from all tropospheric NO₂ observations ($\mathbf{y}_{individual}$) (Hakkarainen et al., 2016; Hakkarainen et al., 2019; Mustafa et al., 2021). The formulation of this method is expressed as:

$$\mathbf{y}_{anomaly} = \mathbf{y}_{individual} - \mathbf{y}_{reference} \quad (3)$$

In this study, we take the average of all **NO₂ VCD_{trop}** from 2005 to 2020 (i.e., the 16-year mean) as the reference value. The MLR model for each city is explained as:

$$\mathbf{y} = \beta_0 + \sum_{k=1}^{11} \beta_k \mathbf{x}_k \quad (4)$$

where \mathbf{y} are the regression result for monthly OMI **NO₂ VCD_{trop}** anomalies, β_0 is the intercept, and \mathbf{x}_k ($k \in [1, 11]$) are the meteorological variables. The regression coefficients β_k are calculated

by nonlinear least squares fitting. This MLR model finds the optimal regression result by minimizing the sum of squares of the fitting residual and then solves regression coefficients β_k by the following equation:

$$\beta_k = (\sum \mathbf{x}_k \mathbf{x}_k^T)^{-1} (\sum \mathbf{x}_k \mathbf{y}_k) \quad (5)$$

The regression results \mathbf{y} represent the meteorology induced contributions to the variabilities of $\text{NO}_2 \text{ VCD}_{\text{trop}}$. Since both soil and lighting NO_x are meteorology dependent, the effects of soil and lighting NO_x on NO_2 variability are also attributed to meteorology contribution. The difference \mathbf{y}' between the monthly OMI $\text{NO}_2 \text{ VCD}_{\text{trop}}$ anomalies $\mathbf{y}_{\text{anomaly}}$ and \mathbf{y} calculated as equation (6) represents the portion that cannot be explicitly explained by the meteorological influence.

$$\mathbf{y}' = \mathbf{y}_{\text{anomaly}} - \mathbf{y} \quad (6)$$

By subtracting the meteorological influence from the total NO_2 amounts, the \mathbf{y}' is referred to as the aggregate contribution of anthropogenic emission. Positive \mathbf{y} and \mathbf{y}' indicate that meteorology and anthropogenic emission cause $\text{NO}_2 \text{ VCD}_{\text{trop}}$ above the reference value (i.e., the 16-year mean), respectively. In contrast, negative \mathbf{y} and \mathbf{y}' indicate that meteorology and anthropogenic emission cause $\text{NO}_2 \text{ VCD}_{\text{trop}}$ below the reference value, respectively.

Since the meteorological parameters listed in Table 2 differ in units and magnitudes, which could lead to unstable performance of the model. Therefore, we normalized all meteorological parameters via equation (7) before using them in regression. This normalization pre-processing procedure can also speed up the convergence of the MLR model.

$$\mathbf{z}_k = \frac{\mathbf{x}_k - \mathbf{u}_k}{\sigma_k} \quad (7)$$

where \mathbf{u}_k and σ_k are the average and 1σ standard deviation (STD) of \mathbf{x}_k , and \mathbf{z}_k is the normalized value for parameter \mathbf{x}_k .

3. Temporal-spatial variabilities of $\text{NO}_2 \text{ VCD}_{\text{trop}}$ over the Yangtze River Delta

3.1 Variabilities at provincial level

We present the temporal-spatial distribution of the annual averaged $\text{NO}_2 \text{ VCD}_{\text{trop}}$ over the YRD from 2005 to 2020 in Figure 1. The major pollution areas for $\text{NO}_2 \text{ VCD}_{\text{trop}}$ over the YRD are located in the south of Jiangsu Province and north of Zhejiang Province. In addition, NO_2 pollution in eastern Anhui Province showed an increasing trend during 2005-2013 and became one of the major pollution areas within YRD during 2010-2013. The amplitudes of $\text{NO}_2 \text{ VCD}_{\text{trop}}$ over the YRD showed large year to year variabilities from 2005 to 2020 but spatial extensions of the major pollution areas are almost constant over years. Among all the pollution areas, the heaviest pollution regions are uniformly located in the densely populated and highly industrialized megacities such as Shanghai, Nanjing, Suzhou, Hangzhou, Ningbo, and Hefei.

The annual means and seasonal cycles of $\text{NO}_2 \text{ VCD}_{\text{trop}}$ over the YRD during 2005-2020 at Province or municipality level, i.e., Anhui Province, Jiangsu Province, Zhejiang Province, and Shanghai municipality, are presented in Figure 2. The $\text{NO}_2 \text{ VCD}_{\text{trop}}$ over each province are calculated by averaging all observations within the boundary of each province. For seasonal variability, clear seasonal features over the whole YRD region and each province are observed (Figure 2a): (1) high levels of $\text{NO}_2 \text{ VCD}_{\text{trop}}$ occur in late winter to spring and low levels of $\text{NO}_2 \text{ VCD}_{\text{trop}}$ occur in later summer to autumn; (2) the 1σ STDs in late winter to spring are larger than those in later summer to autumn; and (3) seasonal cycles of $\text{NO}_2 \text{ VCD}_{\text{trop}}$ over Jiangsu, Zhejiang

and the whole YRD region show bimodal patterns, i.e., two seasonal peaks occur around March and December or January, and one seasonal trough occurs around September; but these over Anhui shows a unimodal pattern and don't have the peak around March. The $\text{NO}_2 \text{ VCD}_{\text{trop}}$ present a maximum monthly mean value of (1.93 ± 0.21) , (2.40 ± 0.25) , (1.61 ± 0.16) , and $(1.91 \pm 0.16) \times 10^{16}$ molecules/cm² in January or December over Anhui, Jiangsu, Zhejiang, and the whole YRD region, respectively. The minimum monthly mean values over Anhui, Jiangsu, Zhejiang and the whole YRD region occur in July, with values of (0.35 ± 0.05) , (0.83 ± 0.07) , (0.57 ± 0.06) , and $(0.39 \pm 0.01) \times 10^{16}$ molecules/cm², respectively.

Except for a few anomalies such as the year-to-year decrease in 2005-2006, and the increases in 2016-2017 and 2018-2019, the overall inter annual variabilities of $\text{NO}_2 \text{ VCD}_{\text{trop}}$ over the YRD can be divided into two stages (Fig. 2b). The first stage was from 2005 to 2011, which showed overall increasing trends in $\text{NO}_2 \text{ VCD}_{\text{trop}}$ over the YRD. During 2005 to 2009 of this stage, change rates of $\text{NO}_2 \text{ VCD}_{\text{trop}}$ were less pronounced, where the 2009 relative to 2005 levels have only increased by $(0.33 \pm 0.02) \times 10^{15}$ $(3.96 \pm 0.25) \%$, $(1.05 \pm 0.11) \times 10^{15}$ $(8.55 \pm 0.08) \%$, and $(0.46 \pm 0.03) \times 10^{15}$ molecule/m² $(5.05 \pm 0.32) \%$ over Anhui, Jiangsu and the whole YRD region, respectively, and leveled off over Zhejiang. However, $\text{NO}_2 \text{ VCD}_{\text{trop}}$ in 2011 relative to 2009 showed significantly increments of $(2.88 \pm 0.23) \times 10^{15}$ $(33.78 \pm 2.70) \%$, $(3.81 \pm 0.32) \times 10^{15}$ $(29.01 \pm 2.45) \%$, $(2.08 \pm 0.18) \times 10^{15}$ $(27.97 \pm 2.43) \%$, $(2.10 \pm 0.19) \times 10^{15}$ molecule/m² $(21.59 \pm 1.95) \%$ over Anhui, Jiangsu, Zhejiang and the whole YRD region, respectively. The second stage was from 2011 to 2020, which showed overall decreasing trends in $\text{NO}_2 \text{ VCD}_{\text{trop}}$ over the YRD. The total decrements over Anhui, Jiangsu, Zhejiang and the whole YRD region in 2020 relative to 2011 are $(4.91 \pm 0.39) \times 10^{15}$ $(41.48 \pm 3.30) \%$, $(4.82 \pm 0.31) \times 10^{15}$ $(43.25 \pm 2.72) \%$, $(3.78 \pm 0.36) \times 10^{15}$ $(40.47 \pm 4.12) \%$, $(4.82 \pm 0.35) \times 10^{15}$ molecule/m² $(43.26 \pm 3.07) \%$, respectively.

We have followed the methodology of (Li et al., 2020)) and used the linear regression model to estimate the inter annual trends of $\text{NO}_2 \text{ VCD}_{\text{trop}}$ over the YRD (Table 3). During 2005-2011, inter annual trends of $\text{NO}_2 \text{ VCD}_{\text{trop}}$ over the YRD region and each province spanned a wide range of $(1.74 \pm 0.72) \times 10^{14}$ molecules/cm²·yr⁻¹ ($p=0.02$) to $(5.94 \pm 1.01) \times 10^{14}$ molecules/cm²·yr⁻¹ ($p<0.01$), indicating a regional representative of each dataset. In contrast, inter annual trends of $\text{NO}_2 \text{ VCD}_{\text{trop}}$ over the YRD region and each province from 2011 to 2020 varied over (-4.86 ± 0.49) to $(-8.16 \pm 0.82) \times 10^{14}$ molecules/cm²·yr⁻¹ ($p<0.01$). For the aggregate trends during 2005-2020, $\text{NO}_2 \text{ VCD}_{\text{trop}}$ over the whole YRD region and each province are negative. The largest and lowest decreasing trends are observed in Jiangsu and Anhui, with values of $(-1.92 \pm 0.30) \times 10^{14}$ molecules/cm²·yr⁻¹ ($p<0.01$) and $(-0.92 \pm 0.26) \times 10^{14}$ molecules/cm²·yr⁻¹ ($p<0.01$), respectively.

3.2 Variabilities at megacity level

The annual means and seasonal cycles of $\text{NO}_2 \text{ VCD}_{\text{trop}}$ over the major megacities within YRD during 2005-2020 are presented in Figure 3. Similar to the derivation of provincial level NO_2 , $\text{NO}_2 \text{ VCD}_{\text{trop}}$ over each megacity are calculated by averaging all observations within the boundary of each megacity. The results show that the amplitudes and variabilities of $\text{NO}_2 \text{ VCD}_{\text{trop}}$ at megacity level are basically coincident with those at the corresponding provincial levels. Overall, the amplitudes and 1 σ STDs of NO_2 seasonal cycles in cold seasons are larger than those in warm seasons, and the inter annual NO_2 variabilities at megacity level can also be divided into two stages, i.e., an overall increasing stage during 2005-2011 and a decreasing stage during 2011-2020. As a

result, it is feasible to select these major megacities as representatives for mapping the drivers of NO₂ variabilities over the YRD.

Specifically, megacity level of $\text{NO}_2 \text{ VCD}_{\text{trop}}$ show seasonal maxima in December and seasonal minima in July. Seasonal maxima over Hefei, Shanghai, Nanjing, Suzhou, Hangzhou, and Ningbo are (2.03 ± 0.15) , (2.80 ± 0.23) , (2.62 ± 0.25) , (2.66 ± 0.16) , (1.83 ± 0.18) , and $(2.27 \pm 0.21) \times 10^{16}$ molecules/cm², and seasonal minima are (0.34 ± 0.04) , (0.83 ± 0.11) , (0.58 ± 0.06) , (0.62 ± 0.05) , (0.32 ± 0.02) , and $(0.38 \pm 0.03) \times 10^{16}$ molecules/cm², respectively. The seasonal maxima are on average $(82.27 \pm 2.34) \%$, $(67.19 \pm 1.56) \%$, $(71.06 \pm 2.32) \%$, $(83.33 \pm 3.05) \%$, $(77.62 \pm 2.89) \%$, and $(70.84 \pm 2.76) \%$ higher than the seasonal minima over respective megacity. As commonly observed, the seasonal variability of $\text{NO}_2 \text{ VCD}_{\text{trop}}$ with respect to their annual means spanned a wide range of -55.1% to 103.5% depending on season and measurement time (Figure 3a).

The $\text{NO}_2 \text{ VCD}_{\text{trop}}$ in all megacities show the maximum values in 2011, where the maximum values over Hefei, Shanghai, Suzhou, Ningbo, Nanjing and Hangzhou are (1.41 ± 0.25) , (2.18 ± 0.23) , (1.81 ± 0.17) , (1.39 ± 0.12) , (1.88 ± 0.18) and $(1.19 \pm 0.14) \times 10^{16}$ molecules/cm², respectively (Figure 3b). In terms of the increments relative to the 2005 levels, Hefei and Shanghai from 2005 to 2011 have the largest and lowest increments of $(5.37 \pm 0.51) \times 10^{15}$ molecules/cm² $(61.77 \pm 5.87) \%$ and $(2.62 \pm 0.27) \times 10^{15}$ molecules /cm² $(14.68 \pm 1.51) \%$, respectively. The increments over other cities varied over $(3.31 \pm 0.32) \times 10^{15}$ molecules /cm² $(31.20 \pm 3.02) \%$ to $(5.21 \pm 0.41) \times 10^{15}$ molecules/cm² $(38.40 \pm 3.02) \%$. In terms of the decrements relative to the 2011 levels, Shanghai and Hangzhou from 2011 to 2020 have the largest and lowest decrements of $(9.77 \pm 0.82) \times 10^{15}$ molecules/cm² $(46.89 \pm 3.94) \%$ and $(5.28 \pm 0.45) \times 10^{15}$ molecules/cm² $(45.43 \pm 3.87) \%$, respectively. The decrements over other cities are also evident and varied over $(6.33 \pm 0.58) \times 10^{15}$ molecules/cm² $(45.53 \pm 4.18) \%$ to $(9.05 \pm 0.98) \times 10^{15}$ molecules/cm² $(48.12 \pm 5.21) \%$. A few anomalies are also observed in some megacities and are in good agreement with the corresponding provincial levels. For example, $\text{NO}_2 \text{ VCD}_{\text{trop}}$ over Hefei and Suzhou had increased by $(0.09 \pm 0.01) \times 10^{15}$ molecules/cm² $(0.77 \pm 0.09) \%$ and $(0.80 \pm 0.07) \times 10^{15}$ molecules/cm² $(4.90 \pm 0.43) \%$ in 2013 relative to 2012 levels, respectively. In addition, $\text{NO}_2 \text{ VCD}_{\text{trop}}$ over Hefei, Shanghai, Nanjing, Hangzhou, and Suzhou had increased by $(0.65 \pm 0.12) \times 10^{15}$ $(8.41 \pm 1.55) \%$, $(0.35 \pm 0.02) \times 10^{15}$ $(2.66 \pm 0.15) \%$, $(0.86 \pm 0.18) \times 10^{15}$ $(8.16 \pm 1.71) \%$, $(0.55 \pm 0.08) \times 10^{15}$ $(8.68 \pm 1.26) \%$, and $(0.29 \pm 0.05) \times 10^{15}$ molecules/cm² $(2.52 \pm 0.43) \%$ in 2019 relative to 2018 levels, respectively.

The inter annual trends of $\text{NO}_2 \text{ VCD}_{\text{trop}}$ during 2005-2011 over all cities are positive and span a wide range of (1.91 ± 1.50) to $(6.70 \pm 0.10) \times 10^{14}$ molecules/cm²·yr⁻¹ ($p < 0.01$) (Table 4). In contrast, the inter annual trends of $\text{NO}_2 \text{ VCD}_{\text{trop}}$ during 2011-2020 over all cities are negative. The largest and lowest decreasing trends are observed in Nanjing and Hangzhou, with values of (-11.01 ± 0.90) and $(-6.31 \pm 0.71) \times 10^{14}$ molecules/cm²·yr⁻¹ ($p < 0.01$), respectively. For the aggregate trends during 2005-2020, $\text{NO}_2 \text{ VCD}_{\text{trop}}$ over all cities are negative. The largest and lowest decreasing trends are observed in Shanghai and Hefei, with values of $(-4.58 \pm 0.43) \times 10^{14}$ molecules/cm²·yr⁻¹ ($p < 0.01$) and $(-0.30 \pm 3.43) \times 10^{14}$ molecules/cm²·yr⁻¹ ($p = 0.385$), respectively.

3.3 Comparisons with the CNMEC data

In order to investigate if satellite column measurements can represent the near surface variabilities, we have compared the OMI $\text{NO}_2 \text{ VCD}_{\text{trop}}$ data over the 6 megacities within the YRD with the ground level NO₂ data provided by the CNMEC (Figure 4). The comparisons over all

megacities were performed on monthly basis between June 2014 and December 2020. Ground level NO_2 concentrations were taken as the average of all CNMEC stations in each city. The NO_2 VCD_{trop} values were taken as the average of all OMI observed grids within the scope of each city. Considering the overpass time of OMI is at about 13:30 LT, we only average the ground level NO_2 data between 13:00 and 14:00 LT for comparison, which ensures that the temporal differences between the CNMEC and OMI dataset are all within ± 30 minutes. With these rules, there are over 700 matching samples in each city available for comparison.

Correlation plots of OMI NO_2 VCD_{trop} data against the CNMEC ground level NO_2 measurements are shown in Figure 4. The results show that the NO_2 variabilities observed by OMI and the CNMEC are in good agreement over all megacities, with correlation coefficients (r^2) of 0.88, 0.81, 0.89, 0.88, 0.86 and 0.83 for Hangzhou, Hefei, Nanjing, Ningbo, Shanghai, and Suzhou, respectively. The discrepancies between OMI and CNMEC data can be mainly attributed to their differences in temporal-spatial resolutions. OMI averages NO_2 concentration at about 13:30 LT over a large coverage due to its relatively coarse spatial resolution (Wallace and Kanaroglou, 2009; Zheng et al., 2014). The CNMEC data represent the averaged point concentrations between 13:00 and 14:00 LT around the measurement site. NO_2 is a short lifetime species and is characterized by large temporal-spatial variabilities. Any temporal-spatial inhomogeneity in NO_2 concentration could affect the comparison (Meng et al., 2010; Wallace and Kanaroglou, 2009). Considering above differences, the correlations of the two datasets over all megacities are satisfactory. The tropospheric NO_2 column measurements can be used as representatives of near-surface conditions. As a result, to simplify calculations, we only use ground-level meteorological data for MLR regression.

Over polluted atmosphere, the NO_2 column measurements can be used as representative of near-surface conditions because tropospheric NO_2 has a vertical distribution that is heavily weighted toward the surface (Kharol et al., 2015; Zhang et al., 2017; Duncan et al., 2016; Duncan et al., 2013; Kramer et al., 2008). Many studies have taken advantage of this favourable vertical distribution of NO_2 to derive surface emissions of NO_2 from space (Silvern et al., 2019; Boersma et al., 2009; Streets et al., 2013; Anand and Monks, 2017; Lu et al., 2015; Ghude et al., 2013; Cooper et al., 2020). Meanwhile, the use of NO_2 column measurements to explore tropospheric O_3 sensitivities has been the subject of several past studies, which disclosed that this diagnosis of O_3 production rate (PO_3) is consistent with the findings of surface photochemistry (Jin et al., 2017; Jin and Holloway, 2015; Sun et al., 2018; Yin et al., 2021b; Souri et al., 2017; Sun et al., 2021b; Jin et al., 2020; Choi and Souri, 2015; Schroeder et al., 2017; Baruah et al., 2021).

4 Implications and drivers

We incorporate the 11 meteorological parameters listed in Table 2 into the MLR model to fit the time series of monthly averaged NO_2 VCD_{trop} from 2005 to 2020 over the 6 megacities within the YRD (Figure S1). Correlation plots of the MLR regression results and the satellite tropospheric NO_2 data are shown in Figure 5. The results show that the MLR model can well reproduce the seasonal variabilities of tropospheric NO_2 VCDs over each city with correlation coefficients of 0.85 to 0.90. We separate the contributions of meteorology and anthropogenic emission to the NO_2 variability over the 6 megacities with the methodology described in section 2.3. Figure 6 shows monthly averaged tropospheric NO_2 VCDs along with the meteorological-driven contributions and the anthropogenic-driven contributions in each city. Figure 7 is the same as Figure 6, but the statistics are based on annual average.

4.1 Drivers of seasonal cycles of $\text{NO}_2 \text{VCD}_{\text{trop}}$

As shown in Figure 6 for all megacities, the seasonal variabilities of meteorological contributions are consistent with those of $\text{NO}_2 \text{VCD}_{\text{trop}}$ except the period from February to March, and the anthropogenic contributions varied around zero throughout the year except in December and February. This means that the seasonal variabilities of tropospheric NO_2 over the YRD are mainly determined by meteorology (81.01% - 83.91%) and also influenced by anthropogenic emission in December and February. Meteorological contributions are larger than zero in winter and lower than zero in summer, indicating that meteorology increases NO_2 level in winter and decreases NO_2 level in summer. This contrast in meteorological contribution is associated with the seasonal cycle of temperature. Similarly, anthropogenic contributions are larger than zero in December and lower than zero in February, representing anthropogenic emission increases NO_2 level in December and decreases NO_2 level in February. The enhanced anthropogenic contributions in December are mainly attributed to more extensive anthropogenic activities such as residential heating in megacities in this period which usually results in more anthropogenic NO_2 emission due to the increase in energy and fuel consumptions. The decreased anthropogenic contributions in February are attributed to the Spring Festival. We elaborate the analysis as below.

As shown in Figure S2, the vast majorities of meteorological contributions over all megacities are from temperature and additional minor contributions over some cities such as Nanjing, Shanghai, and Suzhou are attributed to relative humidity, pressure, or surface incoming shortwave flux (SWGDN) (Agudelo-Castaneda et al., 2014; Parra et al., 2009). Significant negative correlations between temperature and $\text{NO}_2 \text{VCD}_{\text{trop}}$ are observed in all megacities (Figure S3, Table 5). Higher temperature tends to decrease $\text{NO}_2 \text{VCD}_{\text{trop}}$ and vice versa. This is because higher temperature conditions could accelerate the chemical reaction that destructs NO_2 in the troposphere (Pearce et al., 2011; Yin et al., 2021a). In addition, surface pressure shows high positive and both surface relative humidity and SWGDN show negative correlations with $\text{NO}_2 \text{VCD}_{\text{trop}}$, but their contribution levels are much lower than the temperature. All other meteorological variables only have weak correlations with $\text{NO}_2 \text{VCD}_{\text{trop}}$ (Table 5).

In all cities except Hefei, there is a significant increase in NO_2 level from February to March. The maximum and minimum increments occur in Shanghai and Nanjing, with values of $(3.28 \pm 0.29) \times 10^{15}$ molecules/cm² (16.37 ± 1.45 %) and $(0.47 \pm 0.05) \times 10^{15}$ molecules/cm² (2.60 ± 0.28 %), respectively. In contrast, the meteorological contributions show decreased change rates in the same period. As a result, this increase in NO_2 level from February to March could be attributed to anthropogenic emission rather than meteorology. Indeed, anthropogenic contributions show significant increases of (3.95 ± 0.32) to $(6.53 \pm 0.55) \times 10^{15}$ molecules/cm² over all megacities from February to March. The most important festival in China-the Spring Festival-typically occurs in February, when a large number of migrants in megacities return to their hometowns for holiday and most industrial productions are shut down, which could cause significant reductions in anthropogenic emission. In March, these migrants get back to work and all industrial enterprises resumed productions, which could cause a rebound in anthropogenic emission. The seasonal maxima of NO_2 in March are not observed in Hefei is because the anthropogenic emission induced increases are offset by meteorology induced decreases.

2020 is a special year compared to all other years, when a large-scale lockdown occurred in February and some regional travel restrictions occasionally occurred in other seasons across China due to COVID-19 disease. In the comparison, we removed all NO_2 measurements in 2020 to

eliminate the influence of COVID-19. The monthly averaged $\text{NO}_2 \text{VCD}_{\text{trop}}$ from 2005 to 2019 along with the meteorological contributions and the anthropogenic contributions in each city are shown in Figure S4. Figure S5 and Figure S6 are the same as Figure 2 and Figure 3, respectively, but for 2011 to 2019. We obtained the same conclusion as that from Figure 6, indicating the drivers of seasonal cycles of $\text{NO}_2 \text{VCD}_{\text{trop}}$ deduced above are consistent over years.

4.2 Drivers of inter annual variabilities of $\text{NO}_2 \text{VCD}_{\text{trop}}$

As shown in Figure 7 for all megacities, the inter annual variabilities of anthropogenic contributions are in good agreement with those of $\text{NO}_2 \text{VCD}_{\text{trop}}$, indicating inter annual variabilities of $\text{NO}_2 \text{VCD}_{\text{trop}}$ are mainly driven by anthropogenic emission. The same as those of $\text{NO}_2 \text{VCD}_{\text{trop}}$, the inter annual anthropogenic contributions over each city can also be divided into two stages, i.e., an overall increasing stage during 2005–2011 and a decreasing stage during 2011–2020. For the first stage (2005–2011), anthropogenic contributions account for 84.72%, 92.96%, 93.52%, 79.06%, 97.12%, and 90.21% of the increases in $\text{NO}_2 \text{VCD}_{\text{trop}}$, while meteorological contributions account for 15.28%, 7.04%, 6.48%, 20.94%, 2.88%, and 9.79% over Hangzhou, Hefei, Nanjing, Ningbo, Shanghai, and Suzhou, respectively. The annual averaged meteorological contributions over each city varied around zero in all years except few anomalies in some years. For example, meteorological contributions over all cities are larger than zero in 2005 and 2011 but lower than zero after 2014. Pronounced anomalies include the enhancements occurred in 2011 in all cities and the decrements in 2015 over Suzhou, in 2018 over Hangzhou, and in 2016 over other cities. All these anomalies in meteorological contributions are highly correlated with temperature anomalies (Figure S7). As shown in Figure S8 and S9, the temperature in all cities is lower than the reference value (i.e., the 16-year mean) in 2005 and 2011 and larger than the reference value after 2014. As a result, in addition to anthropogenic emission, the NO_2 enhancements in 2011 are partly attributed to the lower temperature in this year. Meanwhile, higher temperature in YRD region in recent years favors the decrease in $\text{NO}_2 \text{VCD}_{\text{trop}}$. For the second stage (2011–2020), anthropogenic contributions account for 70.15 %, 65.22 %, 66.97 %, 73.45 %, 74.43 %, and 73.84 % of the decreases in $\text{NO}_2 \text{VCD}_{\text{trop}}$, while meteorological contributions account for 29.85%, 34.78%, 33.03 %, 26.55 %, 25.57 %, and 26.16 % over Hangzhou, Hefei, Nanjing, Ningbo, Shanghai, and Suzhou, respectively.

Since anthropogenic NO_2 emissions are highly related to economic and industrial activities (Lin and McElroy, 2011; Russell et al., 2012; Vrekoussis et al., 2013; Guerriero et al., 2016), to understand the inter annual variabilities of $\text{NO}_2 \text{VCD}_{\text{trop}}$, we have investigated the inter annual variabilities of Gross Domestic Product (GDP) over the YRD from primary sector, secondary sector and tertiary sector (<http://www.stats.gov.cn/>, last accessed: 1 August, 2021) from 2005 to 2020. The primary sector includes agriculture, forestry, animal husbandry, and fishery; The secondary industry includes mining, manufacturing, power, heat, gas and water production and supply, and construction; The tertiary industry, namely the service industry, refers to all industries excluded the primary industry and the secondary industry. The secondary industry is more related to energy and fuel consumptions, and it thus dominates the anthropogenic NO_2 emission. Figure S10 shows the time series of GDP over the YRD from 2005 to 2020 and Figure S11 is the same as Figure S10 but for year-to-year increment, i.e., the increase in GDP at a given year relative to its previous year. The results show that the GDP of each province within the YRD increased over time starting from 2005 but the relative contribution of each industry sector is different from year to year. The primary

sector-related GDP is relatively constant, but both the secondary sector and tertiary sector related GDPs show significant increasing trends from 2005 to 2020.

During 2009 to 2011, the GDPs have increased significantly by 198.45, 483.86, 656.40, and 327.05 billion yuan over Shanghai, Zhejiang, Jiangsu, and Anhui, where the secondary sector contributions account for 46.50%, 53.64%, 48.99%, and 60.34% respectively. Before 2011, much of China's economic growths still rely on the high-carbon fossil energy system and efforts to control atmospheric pollution were relatively small. These significant increases in GDP could cause significant increases in anthropogenic NO₂ emission. After 2011, China has implemented a series of clean air measures to tackle air pollution across China. These measures include the reduction of industrial pollutant emissions, the adjustment of industrial structure and energy mix, and other compulsive policies (China State Council, 2013). (Zheng et al., 2018a) have estimated China's anthropogenic emission trends from 2010 to 2017 with the bottom-up emission inventory. (Zheng et al., 2018a) found that, as the consequence of clean air measures, anthropogenic NO_x emission across China during 2010–2017 have been decreased by 17%. In Figure S12, we further analyzed the variabilities of NO_x emissions over the YRD region from 2008 to 2017 by category provided by the Multi-resolution Emission Inventory for China (MEIC) inventory, including motor vehicle emissions, major industrial emissions, resident emissions and power emissions (<http://meicmodel.org>, last accessed: February 25, 2022) (Li et al., 2017; Zheng et al., 2018a). The results show that the decreases in Tro NO₂ over the YRD during 2011 to 2013 are attributed to the reductions of industrial and power emissions, during 2013 to 2014 are mainly attributed to the reductions of motor vehicle emissions and power emissions, and after 2014 are attributed to the reductions of motor vehicle emissions, power emissions and industrial emissions.

Although the total GDPs over all megacities are still increasing over time after 2011, much of these increases are from the tertiary sector, indicating the effectiveness of the adjustment of industrial structure and energy mix. The largest anthropogenic NO₂ producer from the tertiary sector is attributed to the transportation industry including such as traffic and cargo transport, etc. Chinese government had implemented stringent restrictions on vehicle exhaust emissions after 2011 (Ministry of Ecology and Environment of the People's Republic of China, 2016, 2011). For example, Chinese government implemented the fourth and the fifth national motor vehicle pollutant emissions standards in 2011 and 2018, respectively, which mandate 30% and 60% reductions in vehicle NO_x emissions relative to the third national standard (Ministry of Ecology and Environment of the People's Republic of China, 2007, 2018). These stringent measures could significantly reduce anthropogenic NO₂ emission from the tertiary sector. Overall, the decreasing trends in NO₂ VCD_{trop} from 2011 to 2020 over all megacities within the YRD are mainly attributed to the stringent clean air measures in this period which either adjust high energy industrial structure toward low energy industrial structure or directly reduce pollutant emissions from different industrial sectors.

5 Conclusions

In this study, we have quantified the long-term variabilities and the underlying drivers of NO₂ VCD_{trop} from 2005-2020 over the Yangtze River Delta (YRD) by OMI LV3 NO₂ data product and MLR regressions. The major pollution areas for NO₂ VCD_{trop} over the YRD are located in the south of Jiangsu Province and north of Zhejiang Province. In addition, NO₂ pollution in eastern Anhui Province showed an increasing trend during 2005-2013 and became one of the major pollution areas

within YRD during 2010-2013. The amplitudes of $\text{NO}_2 \text{ VCD}_{\text{trop}}$ over the YRD showed large year to year variabilities from 2005 to 2020 but spatial extensions of the major pollution areas are almost constant over years. Among all the pollution areas, the heaviest pollution regions are uniformly located in the densely populated and highly industrialized megacities such as Shanghai, Nanjing, Suzhou, Hangzhou, Ningbo, and Hefei. For six megacities the space borne tropospheric results have been compared to surface in-situ data, yielding correlation coefficients between 0.8 and 0.9.

Clear seasonal features and inter annual variabilities of $\text{NO}_2 \text{ VCD}_{\text{trop}}$ over the YRD region are observed. Overall, the amplitudes and 1σ STDs of NO_2 seasonal cycles in cold seasons are larger than those in warm seasons, and the inter annual NO_2 variabilities at megacity level can be divided into two stages, i.e., an overall increasing stage during 2005-2011 and a decreasing stage during 2011-2020. We have used the MLR regressions to quantify the drivers of $\text{NO}_2 \text{ VCD}_{\text{trop}}$ from 2005 to 2020 over all megacities within the YRD. The seasonal cycles of $\text{NO}_2 \text{ VCD}_{\text{trop}}$ over the YRD are mainly driven by meteorology (81.01% - 83.91%) except in winter when anthropogenic emission contributions are also pronounced (16.09% - 18.99%). The inter annual variabilities of $\text{NO}_2 \text{ VCD}_{\text{trop}}$ are mainly driven by anthropogenic emission (69.18% - 81.34%) except in few years such as 2018 which are partly attributed to meteorology anomalies (39.07% - 91.51%).

The increasing trends in $\text{NO}_2 \text{ VCD}_{\text{trop}}$ from 2005 to 2011 over the YRD are mainly attributed to high energy consumption associated with rapid economic growth which cause significant increases in anthropogenic NO_2 emission. The decreasing trends in $\text{NO}_2 \text{ VCD}_{\text{trop}}$ from 2011 to 2020 over the YRD are mainly attributed to the stringent clean air measures in this period which either adjust high energy industrial structure toward low energy industrial structure or directly reduce pollutant emissions from different industrial sectors. This study can not only have improved our knowledge with respect to long term evolutions of economic and social development, anthropogenic emission, and the effectiveness of pollution control measures over the YRD, but also have positive implications for forming future clean air policies in the important region.

Code and data availability. Surface NO_2 measurements over the YRD are from <http://www.cnemc.cn/en/>. The OMI LV3 tropospheric NO_2 satellite data can be obtained from https://acdisc.gesdisc.eosdis.nasa.gov/data/Aura_OMI_Level3/. The Chinese economic data can be obtained from <http://www.stats.gov.cn/>. All other data are available on request of the corresponding author (Youwen Sun, ywsun@aiofm.ac.cn).

Author contributions. HY designed the study and wrote the paper. YS supervised and revised this paper. JN, MP, and CL provided constructive comments.

Competing interests. None.

Acknowledgements. This work is jointly supported by the National Key Research and Development Program of China (No.2019YFC0214802), the Youth Innovation Promotion Association, CAS (No.2019434), and the Sino-German Mobility programme (M-0036).

Table 1. Geolocation, the number of measurement site, and population for the 6 megacities within the YRD. Population statistics are based on the seventh nationwide population census in 2020 provided by National Bureau of Statistics of China.

City	Latitude	Longitude	Number of sites	Altitude (m)	Population (million)
Hangzhou	30.29	120.15	11	41.7	1.19
Hefei	31.85	117.25	10	29.8	0.94
Ningbo	29.87	121.55	9	5.1	0.94
Nanjing	32.04	118.77	9	8.9	0.93
Shanghai	31.23	121.47	10	4.5	2.49
Suzhou	31.30	120.62	8	3.5	1.28

Table 2. Meteorological parameters used in the MLR model.

Parameters	Description	Unit
T _{2m}	2m air temperature	°C
U _{10m}	10m zonal wind	m/s
V _{10m}	10m meridional wind	m/s
PBLH	Planetary boundary layer height	m
TCC	Total cloud area fraction	unitless
Rain	Rainfall	kg·m ² /s
SLP	Sea level pressure	Pa
SWGDN	Surface incoming shortwave flux	W/m ²
RH _{2m}	2m Relative humidity	%
TROPH	Tropospheric layer Height	m

Table 3. Inter annual trends of NO_2 VCD_{trop} over each province within the YRD and the whole YRD region during 2005 to 2011, 2011 to 2020 and 2005 to 2020.

Province	Annual trend (10 ¹⁴ molecule/m ²)		
	2005-2011	2011-2020	2005-2020
YRD	3.69 ± 0.78 (p<0.01)	-6.18 ± 0.52 (p<0.01)	-1.54 ± 0.23 (p<0.01)
Anhui	4.40 ± 0.89 (p<0.01)	-5.93 ± 0.58 (p<0.01)	-0.92 ± 0.26 (p<0.01)
Jiangsu	5.94 ± 1.01 (p<0.01)	-8.16 ± 0.82 (p<0.01)	-1.92 ± 0.30 (p<0.01)
Zhejiang	1.74 ± 0.72 (p=0.02)	-4.86 ± 0.49 (p<0.01)	-1.41 ± 0.22 (p<0.01)

Table 4. Inter annual trends of NO_2 VCD_{trop} over each city within the YRD during 2005 to 2011, 2011 to 2020 and 2005 to 2020.

Province	Annual trend (10 ¹⁴ molecule/m ²)		
	2005-2011	2011-2020	2005-2020
Hangzhou	4.07 ± 1.03 (p<0.01)	-6.31 ± 0.71 (p<0.01)	-1.41 ± 0.30 (p<0.01)
Hefei	6.70 ± 0.11 (p<0.01)	-6.73 ± 0.78 (p<0.01)	-0.30 ± 3.43 (p=0.385)
Nanjing	6.50 ± 1.25 (p<0.01)	-11.01 ± 0.90 (p<0.01)	-2.19 ± 0.39 (p<0.01)
Ningbo	3.79 ± 1.16 (p<0.01)	-7.16 ± 0.81 (p<0.01)	-2.51 ± 0.35 (p<0.01)
Shanghai	1.91 ± 1.50 (p=0.204)	-9.91 ± 0.97 (p<0.01)	-4.58 ± 0.43 (p<0.01)
Suzhou	5.84 ± 0.12 (p<0.01)	-7.16 ± 0.81 (p<0.01)	-2.32 ± 0.35 (p<0.01)

Table 5. Correlations of monthly averaged observations against each meteorological parameter from 2005 to 2020.

City	Correlations									
	T _{2m}	U _{10m}	V _{10m}	PBLH	TCC	Rain	SLP	SWGDN	RH _{2m}	TROPH
Hangzhou	-0.81	-0.11	-0.40	-0.43	-0.63	-0.34	0.84	-0.51	-0.78	0.28
Hefei	-0.84	0.02	-0.48	-0.51	-0.57	-0.39	0.83	-0.69	-0.77	0.25
Nanjing	-0.86	0.07	-0.47	-0.45	-0.56	-0.59	0.86	-0.63	-0.83	0.38
Ningbo	-0.84	0.39	-0.71	-0.14	-0.70	-0.47	0.86	-0.54	-0.82	0.07
Shanghai	-0.82	0.59	-0.65	0.08	-0.66	-0.45	0.83	-0.56	-0.83	0.32
Suzhou	-0.87	0.35	-0.59	-0.60	-0.67	-0.59	0.87	-0.72	-0.82	0.45

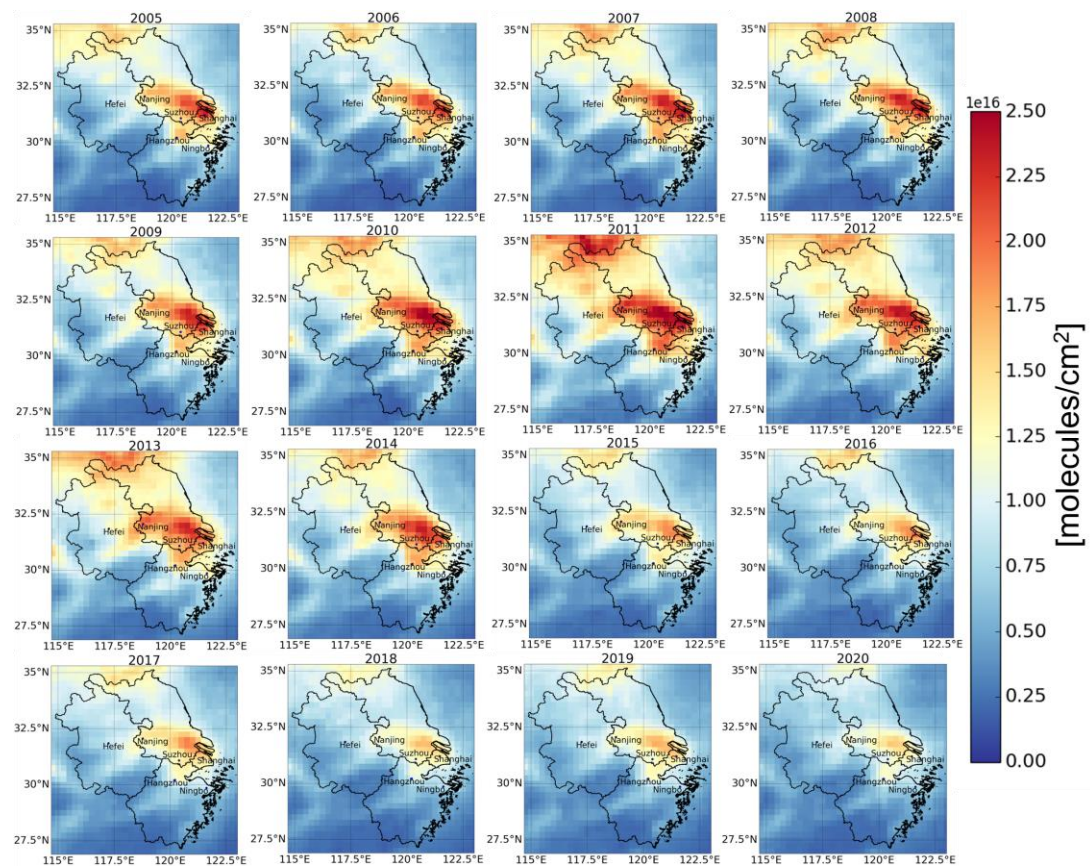


Figure 1. Temporal-spatial variabilities of $\text{NO}_2 \text{VCD}_{\text{trop}}$ provided by OMI satellite over the YRD from 2005 to 2020. The three provinces (Anhui, Jiangsu, Zhejiang) and six key megacities (Hefei, Nanjing, Suzhou, Shanghai, Hangzhou, Ningbo) are marked.

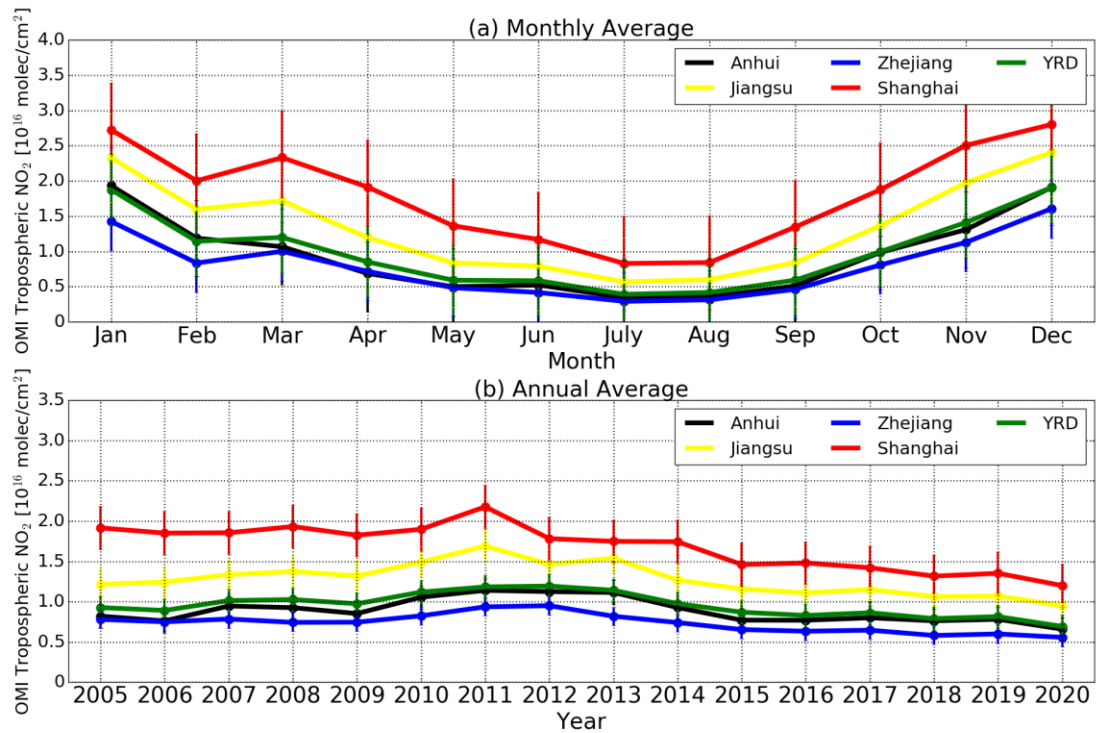


Figure 2. (a) Monthly averaged $\text{NO}_2 \text{ VCD}_{\text{trop}}$ over the whole YRD region (green dots and lines), Anhui Province (black dots and lines), Zhejiang Province (blue dots and lines), and Jiangsu Province (yellow dots and lines). (b) Same as (a) but for annual average. The vertical error bar is 1σ standard variation (STD) within that month or year.

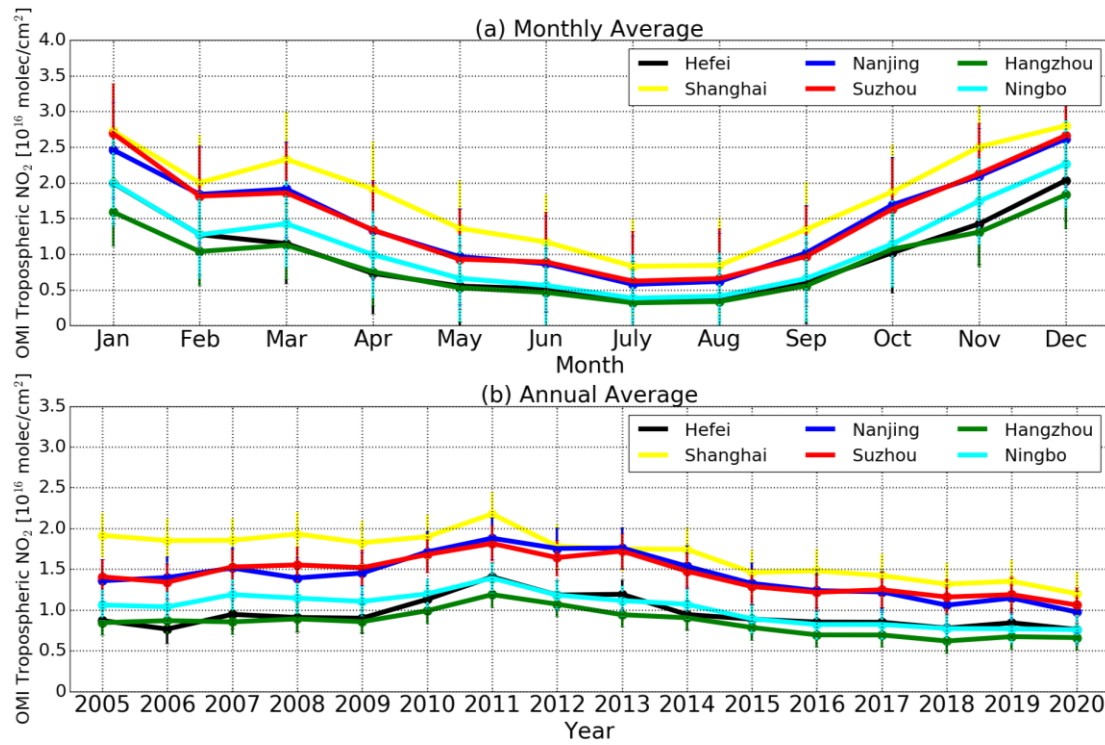


Figure 3. (a) Monthly averaged $\text{NO}_2 \text{VCD}_{\text{trop}}$ over Hefei (black dots and lines), Nanjing (blue dots and lines), Shanghai (yellow dots and lines), Suzhou (red dots and lines), Hangzhou (green dots and lines), and Ningbo (cyan dots and lines). (b) Same as (a) but for annual average. The vertical error bar is 1σ standard variation within that month or year.

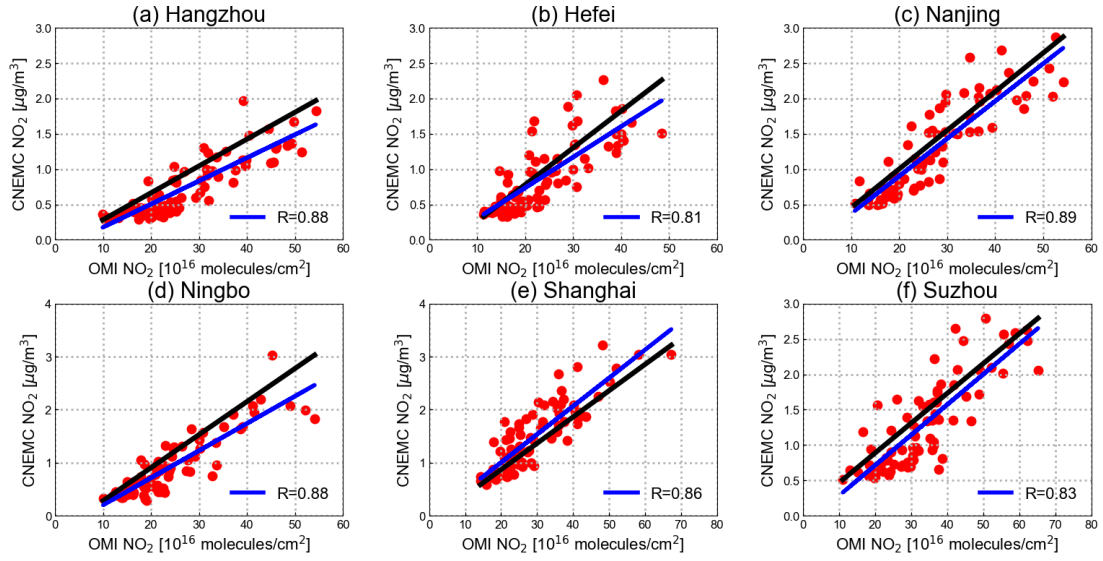


Figure 4. Correlation of OMI $\text{NO}_2 \text{ VCD}_{\text{trop}}$ against ground-level observations data over Hefei, Nanjing, Shanghai, Suzhou, Hangzhou and Ningbo. We fitted both datasets directly without uniform their units, which does not affect the investigation with respect to the agreement of the two datasets in terms of variabilities. Blue lines are linear fitted lines and black lines are one to one line.

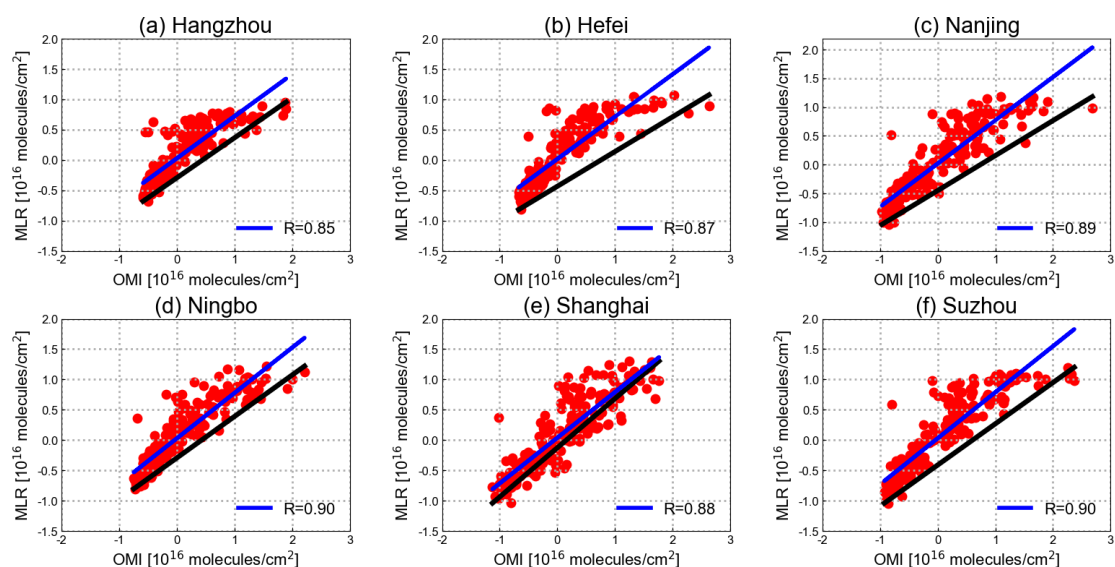


Figure 5. Correlations of OMI $\text{NO}_2 \text{ VCD}_{\text{trop}}$ against the MLR model results over Hefei, Nanjing, Shanghai, Suzhou, Hangzhou, and Ningbo. Blue lines are linear fitted lines and black lines are one to one line.

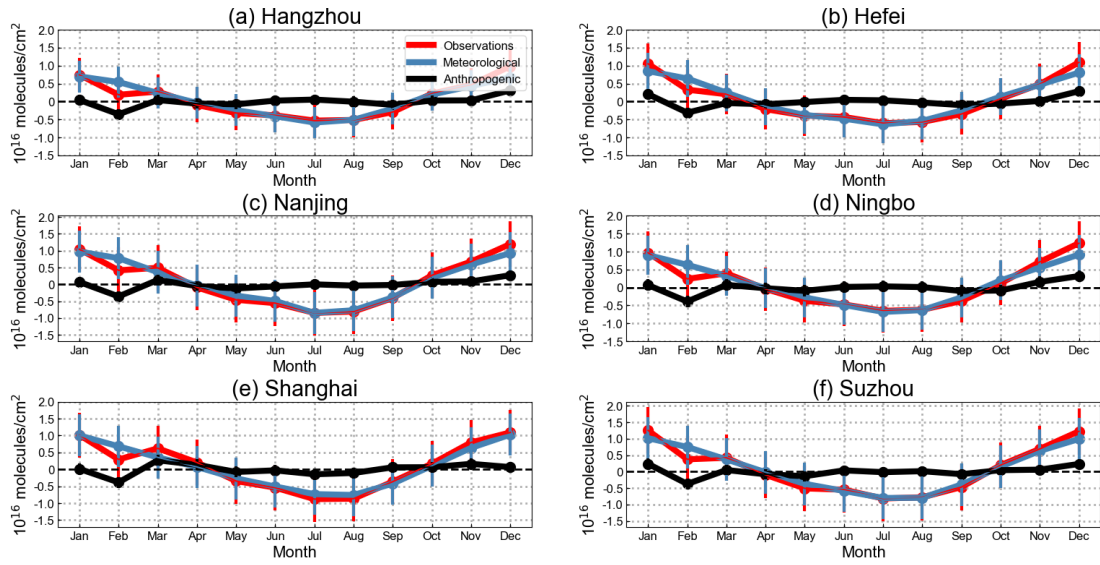


Figure 6. Monthly averaged $\text{NO}_2 \text{VCD}_{\text{trop}}$ (red dots and lines) along with the meteorological-driven portions (blue dots and lines) and the anthropogenic-driven portions (black dots and lines) over each city within the YRD. The vertical error bar is 1σ standard variation (STD) within that month.

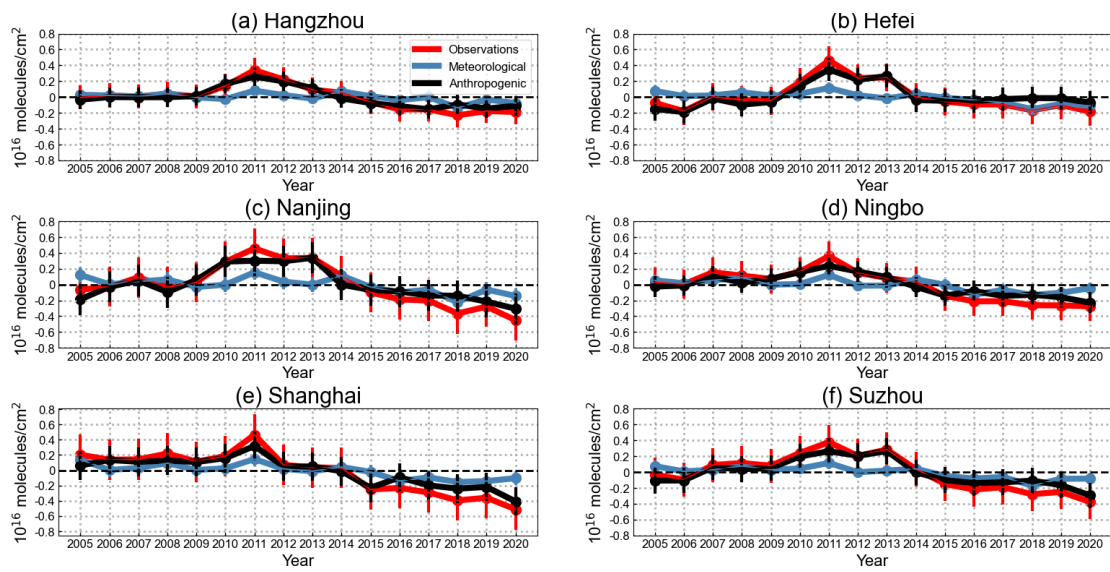


Figure 7. The same as Figure 6 but for annual average.

References

- Agudelo–Castaneda, D. M., Calesso Teixeira, E., and Norte Pereira, F.: Time–series analysis of surface ozone and nitrogen oxides concentrations in an urban area at Brazil, *Atmospheric Pollution Research*, 5, 411–420, <https://doi.org/10.5094/APR.2014.048>, 2014.
- Anand, J. S., and Monks, P. S.: Estimating daily surface NO₂ concentrations from satellite data – a case study over Hong Kong using land use regression models, *Atmos. Chem. Phys.*, 17, 8211–8230, 10.5194/acp-17-8211-2017, 2017.
- Baruah, U. D., Robeson, S. M., Saikia, A., Mili, N., Sung, K., and Chand, P.: Spatio-temporal characterization of tropospheric ozone and its precursor pollutants NO₂ and HCHO over South Asia, *Sci Total Environ*, 151135, <https://doi.org/10.1016/j.scitotenv.2021.151135>, 2021.
- Bechle, M. J., Millet, D. B., and Marshall, J. D.: Remote sensing of exposure to NO₂: Satellite versus ground-based measurement in a large urban area, *Atmos Environ*, 69, 345–353, <https://doi.org/10.1016/j.atmosenv.2012.11.046>, 2013.
- Boersma, K. F., Eskes, H. J., Veefkind, J. P., Brinksma, E. J., van der A, R. J., Sneep, M., van den Oord, G. H. J., Levelt, P. F., Stammes, P., Gleason, J. F., and Bucsela, E. J.: Near-real time retrieval of tropospheric NO₂ from OMI, *Atmos. Chem. Phys.*, 7, 2103–2118, 10.5194/acp-7-2103-2007, 2007.
- Boersma, K. F., Jacob, D. J., Trainic, M., Rudich, Y., DeSmedt, I., Dirksen, R., and Eskes, H. J.: Validation of urban NO₂ concentrations and their diurnal and seasonal variations observed from the SCIAMACHY and OMI sensors using in situ surface measurements in Israeli cities, *Atmos. Chem. Phys.*, 9, 3867–3879, 10.5194/acp-9-3867-2009, 2009.
- Boersma, K. F., Eskes, H. J., Dirksen, R. J., van der A, R. J., Veefkind, J. P., Stammes, P., Huijnen, V., Kleipool, Q. L., Sneep, M., Claas, J., Leitão, J., Richter, A., Zhou, Y., and Brunner, D.: An improved tropospheric NO₂ column retrieval algorithm for the Ozone Monitoring Instrument, *Atmos. Meas. Tech.*, 4, 1905–1928, 10.5194/amt-4-1905-2011, 2011.
- Bond, D. W., Zhang, R., Tie, X., Brasseur, G., Huffman, G., Orville, R. E., and Boccippio, D. J.: NO_x production by lightning over the continental United States, *Journal of Geophysical Research: Atmospheres*, 106, 27701–27710, <https://doi.org/10.1029/2000JD000191>, 2001.
- Browne, E. C., Min, K. E., Wooldridge, P. J., Apel, E., Blake, D. R., Brune, W. H., Cantrell, C. A., Cubison, M. J., Diskin, G. S., Jimenez, J. L., Weinheimer, A. J., Wennberg, P. O., Wisthaler, A., and Cohen, R. C.: Observations of total RONO₂ over the boreal forest: NO_x sinks and HNO₃ sources, *Atmos. Chem. Phys.*, 13, 4543–4562, 10.5194/acp-13-4543-2013, 2013.
- Bucsela, E. J., Krotkov, N. A., Celarier, E. A., Lamsal, L. N., Swartz, W. H., Bhartia, P. K., Boersma, K. F., Veefkind, J. P., Gleason, J. F., and Pickering, K. E.: A new stratospheric and tropospheric NO₂ retrieval algorithm for nadir-viewing satellite instruments: applications to OMI, *Atmos. Meas. Tech.*, 6, 2607–2626, 10.5194/amt-6-2607-2013, 2013.
- Carvalho, D.: An Assessment of NASA’s GMAO MERRA-2 Reanalysis Surface Winds, *J Climate*, 32, 8261–8281, 10.1175/JCLI-D-19-0199.1, 2019.
- Cheng, M. M., Jiang, H., and Guo, Z.: Evaluation of long-term tropospheric NO₂ columns and the effect of different ecosystem in Yangtze River Delta, *Procedia Environmental Sciences*, 13, 1045–1056, <https://doi.org/10.1016/j.proenv.2012.01.098>, 2012.
- Chi, Y., Fan, M., Zhao, C., Sun, L., Yang, Y., Yang, X., and Tao, J.: Ground-level NO₂ concentration estimation based on OMI tropospheric NO₂ and its spatiotemporal characteristics in typical regions of China, *Atmos Res*, 264, 105821, <https://doi.org/10.1016/j.atmosres.2021.105821>, 2021.
- China State Council: the Air Pollution Prevention and Control Action Plan,

http://www.gov.cn/zhengce/content/2013-09/13/content_4561.htm, 2013.

Choi, Y., and Souri, A. H.: Chemical condition and surface ozone in large cities of Texas during the last decade: Observational evidence from OMI, CAMS, and model analysis, *Remote Sens Environ*, 168, 90-101, 2015.

Cooper, M. J., Martin, R. V., McLinden, C. A., and Brook, J. R.: Inferring ground-level nitrogen dioxide concentrations at fine spatial resolution applied to the TROPOMI satellite instrument, *Environ Res Lett*, 15, 104013, [10.1088/1748-9326/aba3a5](https://doi.org/10.1088/1748-9326/aba3a5), 2020.

Duncan, B. N., Yoshida, Y., de Foy, B., Lamsal, L. N., Streets, D. G., Lu, Z., Pickering, K. E., and Krotkov, N. A.: The observed response of Ozone Monitoring Instrument (OMI) NO₂ columns to NO_x emission controls on power plants in the United States: 2005–2011, *Atmos Environ*, 81, 102–111, <https://doi.org/10.1016/j.atmosenv.2013.08.068>, 2013.

Duncan, B. N., Lamsal, L. N., Thompson, A. M., Yoshida, Y., Lu, Z., Streets, D. G., Hurwitz, M. M., and Pickering, K. E.: A space-based, high-resolution view of notable changes in urban NO_x pollution around the world (2005–2014), *Journal of Geophysical Research: Atmospheres*, 121, 976–996, <https://doi.org/10.1002/2015JD024121>, 2016.

Geddes, J. A., Murphy, J. G., O'Brien, J. M., and Celarier, E. A.: Biases in long-term NO₂ averages inferred from satellite observations due to cloud selection criteria, *Remote Sens Environ*, 124, 210–216, <https://doi.org/10.1016/j.rse.2012.05.008>, 2012.

Gelaro, R., McCarty, W., Suárez, M. J., Todling, R., Molod, A., Takacs, L., Randles, C. A., Darmenov, A., Bosilovich, M. G., Reichle, R., Wargan, K., Coy, L., Cullather, R., Draper, C., Akella, S., Buchard, V., Conaty, A., da Silva, A. M., Gu, W., Gi-Kong, K., Koster, R., Lucchesi, R., Merkova, D., Nielsen, J. E., Partyka, G., Pawson, S., Putman, W., Rienecker, M., Schubert, S. D., Sienkiewicz, M., and Zhao, B.: The Modern-Era Retrospective Analysis for Research and Applications, Version 2 (MERRA-2), *J Climate*, 30, 5419–5454, <http://dx.doi.org/10.1175/JCLI-D-16-0758.1>", 2017.

Ghude, S. D., Van der A, R. J., Beig, G., Fadnavis, S., and Polade, S. D.: Satellite derived trends in NO₂ over the major global hotspot regions during the past decade and their inter-comparison, *Environmental Pollution*, 157, 1873–1878, <https://doi.org/10.1016/j.envpol.2009.01.013>, 2009.

Ghude, S. D., Pfister, G. G., Jena, C., van der A, R. J., Emmons, L. K., and Kumar, R.: Satellite constraints of nitrogen oxide (NO_x) emissions from India based on OMI observations and WRF-Chem simulations, *Geophys Res Lett*, 40, 423–428, <https://doi.org/10.1002/grl.50065>, 2013.

Goldberg, D. L., Lamsal, L. N., Loughner, C. P., Swartz, W. H., Lu, Z., and Streets, D. G.: A high-resolution and observationally constrained OMI NO₂ satellite retrieval, *Atmos. Chem. Phys.*, 17, 11403–11421, [10.5194/acp-17-11403-2017](https://doi.org/10.5194/acp-17-11403-2017), 2017.

Guerriero, C., Chatzidiakou, L., Cairns, J., and Mumovic, D.: The economic benefits of reducing the levels of nitrogen dioxide (NO₂) near primary schools: The case of London, *Journal of Environmental Management*, 181, 615–622, <https://doi.org/10.1016/j.jenvman.2016.06.039>, 2016.

Hakkarainen, J., Ialongo, I., and Tamminen, J.: Direct space-based observations of anthropogenic CO₂ emission areas from OCO-2, *Geophys Res Lett*, 43, 11,400–411,406, <https://doi.org/10.1002/2016GL070885>, 2016.

Hakkarainen, J., Ialongo, I., Maksyutov, S., and Crisp, D.: Analysis of Four Years of Global XCO₂ Anomalies as Seen by Orbiting Carbon Observatory-2, *Remote Sens-Basel*, 11, 10.3390/rs11070850, 2019.

He, J., Gong, S., Yu, Y., Yu, L., Wu, L., Mao, H., Song, C., Zhao, S., Liu, H., Li, X., and Li, R.: Air pollution characteristics and their relation to meteorological conditions during 2014–2015 in major

Chinese cities, *Environmental Pollution*, 223, 484-496, <https://doi.org/10.1016/j.envpol.2017.01.050>, 2017.

Hilboll, A., Richter, A., and Burrows, J. P.: Long-term changes of tropospheric NO₂ over megacities derived from multiple satellite instruments, *Atmos. Chem. Phys.*, 13, 4145-4169, 10.5194/acp-13-4145-2013, 2013.

Jiang, Z., McDonald, B. C., Worden, H., Worden, J. R., Miyazaki, K., Qu, Z., Henze, D. K., Jones, D. B. A., Arellano, A. F., Fischer, E. V., Zhu, L. Y., and Boersma, K. F.: Unexpected slowdown of US pollutant emission reduction in the past decade, *P Natl Acad Sci USA*, 115, 5099-5104, 2018.

Jin, X., Fiore, A. M., Murray, L. T., Valin, L. C., Lamsal, L. N., Duncan, B., Folkert Boersma, K., De Smedt, I., Abad, G. G., Chance, K., and Tonnesen, G. S.: Evaluating a Space-Based Indicator of Surface Ozone-NO_x-VOC Sensitivity Over Midlatitude Source Regions and Application to Decadal Trends, *Journal of Geophysical Research: Atmospheres*, 122, 10,439-410,461, <https://doi.org/10.1002/2017JD026720>, 2017.

Jin, X., Fiore, A., Boersma, K. F., Smedt, I. D., and Valin, L.: Inferring Changes in Summertime Surface Ozone-NO_x-VOC Chemistry over U.S. Urban Areas from Two Decades of Satellite and Ground-Based Observations, *Environmental Science & Technology*, 54, 6518-6529, 10.1021/acs.est.9b07785, 2020.

Jin, X. M., and Holloway, T.: Spatial and temporal variability of ozone sensitivity over China observed from the Ozone Monitoring Instrument, *J Geophys Res-Atmos*, 120, 7229-7246, 2015.

Kharol, S. K., Martin, R. V., Philip, S., Boys, B., Lamsal, L. N., Jerrett, M., Brauer, M., Crouse, D. L., McLinden, C., and Burnett, R. T.: Assessment of the magnitude and recent trends in satellite-derived ground-level nitrogen dioxide over North America, *Atmos Environ*, 118, 236-245, <https://doi.org/10.1016/j.atmosenv.2015.08.011>, 2015.

Kim, D.-R., Lee, J.-B., Keun Song, C., Kim, S.-Y., Ma, Y.-I., Lee, K.-M., Cha, J.-S., and Lee, S.-D.: Temporal and spatial distribution of tropospheric NO₂ over Northeast Asia using OMI data during the years 2005–2010, *Atmospheric Pollution Research*, 6, 768-776, <https://doi.org/10.5094/APR.2015.085>, 2015.

Kishore Kumar, G., Kishore Kumar, K., Baumgarten, G., and Ramkumar, G.: Validation of MERRA reanalysis upper-level winds over low latitudes with independent rocket sounding data, *J Atmos Sol-Terr Phy*, 123, 48-54, <https://doi.org/10.1016/j.jastp.2014.12.001>, 2015.

Kramer, L. J., Leigh, R. J., Remedios, J. J., and Monks, P. S.: Comparison of OMI and ground-based in situ and MAX-DOAS measurements of tropospheric nitrogen dioxide in an urban area, *Journal of Geophysical Research: Atmospheres*, 113, <https://doi.org/10.1029/2007JD009168>, 2008.

Krotkov, N. A., McLinden, C. A., Li, C., Lamsal, L. N., Celarier, E. A., Marchenko, S. V., Swartz, W. H., Bucsela, E. J., Joiner, J., Duncan, B. N., Boersma, K. F., Veefkind, J. P., Levelt, P. F., Fioletov, V. E., Dickerson, R. R., He, H., Lu, Z., and Streets, D. G.: Aura OMI observations of regional SO₂ and NO₂ pollution changes from 2005 to 2015, *Atmos. Chem. Phys.*, 16, 4605-4629, 10.5194/acp-16-4605-2016, 2016.

Lamsal, L. N., Martin, R. V., van Donkelaar, A., Steinbacher, M., Celarier, E. A., Bucsela, E., Dunlea, E. J., and Pinto, J. P.: Ground-level nitrogen dioxide concentrations inferred from the satellite-borne Ozone Monitoring Instrument, *Journal of Geophysical Research: Atmospheres*, 113, <https://doi.org/10.1029/2007JD009235>, 2008.

Lamsal, L. N., Krotkov, N. A., Celarier, E. A., Swartz, W. H., Pickering, K. E., Bucsela, E. J., Gleason, J. F., Martin, R. V., Philip, S., Irie, H., Cede, A., Herman, J., Weinheimer, A., Szykman, J. J., and Knepp, T. N.: Evaluation of OMI operational standard NO₂ column retrievals using in situ and surface-based

NO₂ observations, *Atmos. Chem. Phys.*, 14, 11587-11609, 10.5194/acp-14-11587-2014, 2014.

Lamsal, L. N., Duncan, B. N., Yoshida, Y., Krotkov, N. A., Pickering, K. E., Streets, D. G., and Lu, Z.: U.S. NO₂ trends (2005–2013): EPA Air Quality System (AQS) data versus improved observations from the Ozone Monitoring Instrument (OMI), *Atmos Environ*, 110, 130-143, <https://doi.org/10.1016/j.atmosenv.2015.03.055>, 2015.

Levelt, P. F., Oord, G. H. J. v. d., Dobber, M. R., Malkki, A., Huib, V., Johan de, V., Stammes, P., Lundell, J. O. V., and Saari, H.: The ozone monitoring instrument, *IEEE Transactions on Geoscience and Remote Sensing*, 44, 1093-1101, 10.1109/TGRS.2006.872333, 2006.

Li, K., Jacob, D. J., Liao, H., Shen, L., Zhang, Q., and Bates, K. H.: Anthropogenic drivers of 2013–2017 trends in summer surface ozone in China, *Proceedings of the National Academy of Sciences*, 116, 422, 10.1073/pnas.1812168116, 2019.

Li, K., Jacob, D. J., Shen, L., Lu, X., De Smedt, I., and Liao, H.: Increases in surface ozone pollution in China from 2013 to 2019: anthropogenic and meteorological influences, *Atmos. Chem. Phys.*, 20, 11423-11433, 10.5194/acp-20-11423-2020, 2020.

Li, M., Liu, H., Geng, G., Hong, C., Liu, F., Song, Y., Tong, D., Zheng, B., Cui, H., Man, H., Zhang, Q., and He, K.: Anthropogenic emission inventories in China: a review, *Natl Sci Rev*, 4, 834-866, 10.1093/nsr/nwx150, 2017.

Li, R., Xu, M., Li, M., Chen, Z., Zhao, N., Gao, B., and Yao, Q.: Identifying the spatiotemporal variations in ozone formation regimes across China from 2005 to 2019 based on polynomial simulation and causality analysis, *Atmos. Chem. Phys.*, 21, 15631-15646, 10.5194/acp-21-15631-2021, 2021.

Lin, C., Lau, A. K. H., Fung, J. C. H., Song, Y., Li, Y., Tao, M., Lu, X., Ma, J., and Lao, X. Q.: Removing the effects of meteorological factors on changes in nitrogen dioxide and ozone concentrations in China from 2013 to 2020, *Sci Total Environ*, 793, 148575, <https://doi.org/10.1016/j.scitotenv.2021.148575>, 2021.

Lin, J., Nielsen, C. P., Zhao, Y., Lei, Y., Liu, Y., and McElroy, M. B.: Recent Changes in Particulate Air Pollution over China Observed from Space and the Ground: Effectiveness of Emission Control, *Environmental Science & Technology*, 44, 7771-7776, 10.1021/es101094t, 2010.

Lin, J. T., and McElroy, M. B.: Detection from space of a reduction in anthropogenic emissions of nitrogen oxides during the Chinese economic downturn, *Atmos. Chem. Phys.*, 11, 8171-8188, 10.5194/acp-11-8171-2011, 2011.

Liu, F., Zhang, Q., van der A, R. J., Zheng, B., Tong, D., Yan, L., Zheng, Y., and He, K.: Recent reduction in NO_x emissions over China: synthesis of satellite observations and emission inventories, *Environ Res Lett*, 11, 114002, 10.1088/1748-9326/11/11/114002, 2016.

Liu, F., Beirle, S., Zhang, Q., van der A, R. J., Zheng, B., Tong, D., and He, K.: NO_x emission trends over Chinese cities estimated from OMI observations during 2005 to 2015, *Atmos. Chem. Phys.*, 17, 9261-9275, 10.5194/acp-17-9261-2017, 2017.

Liu, F., van der A, R. J., Eskes, H., Ding, J., and Mijling, B.: Evaluation of modeling NO₂ concentrations driven by satellite-derived and bottom-up emission inventories using in situ measurements over China, *Atmos. Chem. Phys.*, 18, 4171-4186, 10.5194/acp-18-4171-2018, 2018.

Lu, X., Zhang, L., Chen, Y., Zhou, M., Zheng, B., Li, K., Liu, Y., Lin, J., Fu, T. M., and Zhang, Q.: Exploring 2016–2017 surface ozone pollution over China: source contributions and meteorological influences, *Atmos. Chem. Phys.*, 19, 8339-8361, 10.5194/acp-19-8339-2019, 2019a.

Lu, X., Zhang, L., and Shen, L.: Meteorology and Climate Influences on Tropospheric Ozone: a Review of Natural Sources, Chemistry, and Transport Patterns, *Current Pollution Reports*, 5, 238-260,

10.1007/s40726-019-00118-3, 2019b.

Lu, X., Zhang, L., Wang, X., Gao, M., Li, K., Zhang, Y., Yue, X., and Zhang, Y.: Rapid Increases in Warm-Season Surface Ozone and Resulting Health Impact in China Since 2013, *Environ Sci Tech Let*, 7, 240-247, 10.1021/acs.estlett.0c00171, 2020.

Lu, X., Ye, X., Zhou, M., Zhao, Y., Weng, H., Kong, H., Li, K., Gao, M., Zheng, B., Lin, J., Zhou, F., Zhang, Q., Wu, D., Zhang, L., and Zhang, Y.: The underappreciated role of agricultural soil nitrogen oxide emissions in ozone pollution regulation in North China, *Nature Communications*, 12, 5021, 10.1038/s41467-021-25147-9, 2021.

Lu, Z., Streets, D. G., de Foy, B., Lamsal, L. N., Duncan, B. N., and Xing, J.: Emissions of nitrogen oxides from US urban areas: estimation from Ozone Monitoring Instrument retrievals for 2005–2014, *Atmos. Chem. Phys.*, 15, 10367-10383, 10.5194/acp-15-10367-2015, 2015.

MacIntyre, E. A., Gehring, U., Mölter, A., Fuertes, E., Klümper, C., Krämer, U., Quass, U., Hoffmann, B., Gascon, M., Brunekreef, B., Koppelman, G. H., Beelen, R., Hoek, G., Birk, M., de Jongste, J. C., Smit, H. A., Cyrus, J., Gruzieva, O., Korek, M., Bergström, A., Agius, R. M., de Vocht, F., Simpson, A., Porta, D., Forastiere, F., Badaloni, C., Cesaroni, G., Esplugues, A., Fernández-Somoano, A., Lerxundi, A., Sunyer, J., Cirach, M., Nieuwenhuijsen, M. J., Pershagen, G., and Heinrich, J.: Air pollution and respiratory infections during early childhood: An analysis of 10 European birth cohorts within the ESCAPE project, *Environmental Health Perspectives*, 122, 107-113, 10.1289/ehp.1306755, 2014.

Marchenko, S., Krotkov, N. A., Lamsal, L. N., Celarier, E. A., Swartz, W. H., and Bucsela, E. J.: Revising the slant column density retrieval of nitrogen dioxide observed by the Ozone Monitoring Instrument, *Journal of Geophysical Research: Atmospheres*, 120, 5670-5692, <https://doi.org/10.1002/2014JD022913>, 2015.

Meng, X., Liu, C., Chen, R. J., Sera, F., Vicedo-Cabrera, A. M., Milojevic, A., Guo, Y. M., Tong, S. L., Coelho, M. D. Z. S., Saldiva, P. H. N., Lavigne, E., Correa, P. M., Ortega, N. V., Garcia, S. O., Kysely, J., Urban, A., Orru, H., Maasikmets, M., Jaakkola, J. J. K., Rytö, N., Huber, V., Schneider, A., Katsouyanni, K., Analitis, A., Hashizume, M., Honda, Y., Ng, C. F. S., Nunes, B., Teixeira, J. P., Holobaca, I. H., Fratianni, S., Kim, H., Tobias, A., Iniguez, C., Forsberg, B., Astrom, C., Ragettli, M. S., Guo, Y. L. L., Pan, S. C., Li, S. S., Bell, M. L., Zanobetti, A., Schwartz, J., Wu, T. C., Gasparrini, A., and Kan, H. D.: Short term associations of ambient nitrogen dioxide with daily total, cardiovascular, and respiratory mortality: multilocation analysis in 398 cities, *Bmj-Brit Med J*, 372, 2021.

Meng, Z.-Y., Xu, X.-B., Wang, T., Zhang, X.-Y., Yu, X.-L., Wang, S.-F., Lin, W.-L., Chen, Y.-Z., Jiang, Y.-A., and An, X.-Q.: Ambient sulfur dioxide, nitrogen dioxide, and ammonia at ten background and rural sites in China during 2007–2008, *Atmos Environ*, 44, 2625-2631, <https://doi.org/10.1016/j.atmosenv.2010.04.008>, 2010.

Ministry of Ecology and Environment of the People's Republic of China: Limits and measurement methods for emissions from light-duty vehicles (III , IV), http://www.mee.gov.cn/ywgz/fgbz/bz/bzwb/dqhjbh/dqdywrwpfbz/200707/t20070701_66145.shtml, 2007.

Ministry of Ecology and Environment of the People's Republic of China: Announcement on the implementation of the national phase IV vehicle compression ignition engine and vehicle pollutant emission standards, https://www.mee.gov.cn/gkml/hbb/bgg/201201/t20120110_222376.htm, 2011.

Ministry of Ecology and Environment of the People's Republic of China: Announcement on the implementation of phase V motor vehicle emission standards,, https://www.mee.gov.cn/gkml/hbb/bgg/201601/t20160118_326596.htm, 2016.

Ministry of Ecology and Environment of the People's Republic of China: Limits and measurement methods for emissions from light-duty vehicles (CHINA 5), http://www.mee.gov.cn/ywgz/fgbz/bz/bzwb/dqjhjbh/dqdywrwpfbz/201309/t20130917_260352.shtml, 2018.

Mustafa, F., Bu, L., Wang, Q., Yao, N., Shahzaman, M., Bilal, M., Aslam, R. W., and Iqbal, R.: Neural-network-based estimation of regional-scale anthropogenic CO₂ emissions using an Orbiting Carbon Observatory-2 (OCO-2) dataset over East and West Asia, *Atmos. Meas. Tech.*, 14, 7277-7290, 10.5194/amt-14-7277-2021, 2021.

Parra, M. A., Elustondo, D., Bermejo, R., and Santamaría, J. M.: Ambient air levels of volatile organic compounds (VOC) and nitrogen dioxide (NO₂) in a medium size city in Northern Spain, *Sci Total Environ*, 407, 999-1009, <https://doi.org/10.1016/j.scitotenv.2008.10.032>, 2009.

Pearce, J. L., Beringer, J., Nicholls, N., Hyndman, R. J., and Tapper, N. J.: Quantifying the influence of local meteorology on air quality using generalized additive models, *Atmos Environ*, 45, 1328-1336, <https://doi.org/10.1016/j.atmosenv.2010.11.051>, 2011.

Richter, A., Burrows, J. P., Nüß, H., Granier, C., and Niemeier, U.: Increase in tropospheric nitrogen dioxide over China observed from space, *Nature*, 437, 129-132, 10.1038/nature04092, 2005.

Rotman, D. A., Tannahill, J. R., Kinnison, D. E., Connell, P. S., Bergmann, D., Proctor, D., Rodriguez, J. M., Lin, S. J., Rood, R. B., Prather, M. J., Rasch, P. J., Considine, D. B., Ramaroson, R., and Kawa, S. R.: Global Modeling Initiative assessment model: Model description, integration, and testing of the transport shell, *Journal of Geophysical Research: Atmospheres*, 106, 1669-1691, <https://doi.org/10.1029/2000JD900463>, 2001.

Russell, A. R., Valin, L. C., and Cohen, R. C.: Trends in OMI NO₂ observations over the United States: effects of emission control technology and the economic recession, *Atmos. Chem. Phys.*, 12, 12197-12209, 10.5194/acp-12-12197-2012, 2012.

Schreier, S. F., Peters, E., Richter, A., Lampel, J., Wittrock, F., and Burrows, J. P.: Ship-based MAX-DOAS measurements of tropospheric NO₂ and SO₂ in the South China and Sulu Sea, *Atmos Environ*, 102, 331-343, <https://doi.org/10.1016/j.atmosenv.2014.12.015>, 2015.

Schroeder, J. R., Crawford, J. H., Fried, A., Walega, J., Weinheimer, A., Wisthaler, A., Muller, M., Mikoviny, T., Chen, G., Shook, M., Blake, D. R., and Tonnesen, G. S.: New insights into the column CH₂O/NO₂ ratio as an indicator of near-surface ozone sensitivity, *J Geophys Res-Atmos*, 122, 8885-8907, 2017.

Shaiganfar, R., Beirle, S., Denier van der Gon, H., Jonkers, S., Kuenen, J., Petetin, H., Zhang, Q., Beekmann, M., and Wagner, T.: Estimation of the Paris NO₂ emissions from mobile MAX-DOAS observations and CHIMERE model simulations during the MEGAPOLI campaign using the closed integral method, *Atmos. Chem. Phys.*, 17, 7853-7890, 10.5194/acp-17-7853-2017, 2017.

Silvern, R. F., Jacob, D. J., Mickley, L. J., Sulprizio, M. P., Travis, K. R., Marais, E. A., Cohen, R. C., Laughner, J. L., Choi, S., Joiner, J., and Lamsal, L. N.: Using satellite observations of tropospheric NO₂ columns to infer long-term trends in US NO_x emissions: the importance of accounting for the free tropospheric NO₂ background, *Atmos. Chem. Phys.*, 19, 8863-8878, 10.5194/acp-19-8863-2019, 2019.

Solomon, S., Schmeltekopf, A. L., and Sanders, R. W.: On the interpretation of zenith sky absorption measurements, *Journal of Geophysical Research: Atmospheres*, 92, 8311-8319, <https://doi.org/10.1029/JD092iD07p08311>, 1987.

Song, Z., Fu, D., Zhang, X., Wu, Y., Xia, X., He, J., Han, X., Zhang, R., and Che, H.: Diurnal and seasonal variability of PM_{2.5} and AOD in North China plain: Comparison of MERRA-2 products and ground

measurements, *Atmos Environ*, 191, 70-78, <https://doi.org/10.1016/j.atmosenv.2018.08.012>, 2018.

Souri, A. H., Choi, Y., Jeon, W., Woo, J.-H., Zhang, Q., and Kurokawa, J.-i.: Remote sensing evidence of decadal changes in major tropospheric ozone precursors over East Asia, *Journal of Geophysical Research: Atmospheres*, 122, 2474-2492, <https://doi.org/10.1002/2016JD025663>, 2017.

Streets, D. G., Canty, T., Carmichael, G. R., de Foy, B., Dickerson, R. R., Duncan, B. N., Edwards, D. P., Haynes, J. A., Henze, D. K., Houyoux, M. R., Jacob, D. J., Krotkov, N. A., Lamsal, L. N., Liu, Y., Lu, Z., Martin, R. V., Pfister, G. G., Pinder, R. W., Salawitch, R. J., and Wecht, K. J.: Emissions estimation from satellite retrievals: A review of current capability, *Atmos Environ*, 77, 1011-1042, <https://doi.org/10.1016/j.atmosenv.2013.05.051>, 2013.

Sun, Y., Liu, C., Zhang, L., Palm, M., Notholt, J., Yin, H., Vigouroux, C., Lutsch, E., Wang, W., Shan, C., Blumenstock, T., Nagahama, T., Morino, I., Mahieu, E., Strong, K., Langerock, B., De Mazière, M., Hu, Q., Zhang, H., Petri, C., and Liu, J.: Fourier transform infrared time series of tropospheric HCN in eastern China: seasonality, interannual variability, and source attribution, *Atmos. Chem. Phys.*, 20, 5437-5456, 10.5194/acp-20-5437-2020, 2020.

Sun, Y., Yin, H., Liu, C., Zhang, L., Cheng, Y., Palm, M., Notholt, J., Lu, X., Vigouroux, C., Zheng, B., Wang, W., Jones, N., Shan, C., Qin, M., Tian, Y., Hu, Q., Meng, F., and Liu, J.: Mapping the drivers of formaldehyde (HCHO) variability from 2015 to 2019 over eastern China: insights from Fourier transform infrared observation and GEOS-Chem model simulation, *Atmos. Chem. Phys.*, 21, 6365-6387, 10.5194/acp-21-6365-2021, 2021a.

Sun, Y., Yin, H., Lu, X., Notholt, J., Palm, M., Liu, C., Tian, Y., and Zheng, B.: The drivers and health risks of the unexpected surface ozone enhancements over the Sichuan basin, China in 2020, *Atmos. Chem. Phys. Discuss.*, 2021, 1-29, 10.5194/acp-2021-664, 2021b.

Sun, Y., Yin, H., Cheng, Y., Zhang, Q., Zheng, B., Notholt, J., Lu, X., Liu, C., Tian, Y., and Liu, J.: Quantifying variability, source, and transport of CO in the urban areas over the Himalayas and Tibetan Plateau, *Atmos. Chem. Phys.*, 21, 9201-9222, 10.5194/acp-21-9201-2021, 2021c.

Sun, Y. W., Liu, C., Palm, M., Vigouroux, C., Notholt, J., Hui, Q. H., Jones, N., Wang, W., Su, W. J., Zhang, W. Q., Shan, C. G., Tian, Y., Xu, X. W., De Mazière, M., Zhou, M. Q., and Liu, J. G.: Ozone seasonal evolution and photochemical production regime in the polluted troposphere in eastern China derived from high-resolution Fourier transform spectrometry (FTS) observations, *Atmos Chem Phys*, 18, 14569-14583, 2018.

Tao, Y., Huang, W., Huang, X., Zhong, L., Lu, S. E., Li, Y., Dai, L., Zhang, Y., and Zhu, T.: Estimated acute effects of ambient ozone and nitrogen dioxide on mortality in the Pearl River Delta of southern China, *Environmental Health Perspectives*, 120, 393-398, 10.1289/ehp.1103715, 2012.

van Geffen, J. H. G. M., Boersma, K. F., Van Roozendaal, M., Hendrick, F., Mahieu, E., De Smedt, I., Sneep, M., and Veefkind, J. P.: Improved spectral fitting of nitrogen dioxide from OMI in the 405–465 nm window, *Atmos. Meas. Tech.*, 8, 1685-1699, 10.5194/amt-8-1685-2015, 2015.

Vrekoussis, M., Richter, A., Hilboll, A., Burrows, J. P., Gerasopoulos, E., Lelieveld, J., Barrie, L., Zerefos, C., and Mihalopoulos, N.: Economic crisis detected from space: Air quality observations over Athens/Greece, *Geophys Res Lett*, 40, 458-463, <https://doi.org/10.1002/grl.50118>, 2013.

Wallace, J., and Kanaroglou, P.: The sensitivity of OMI-derived nitrogen dioxide to boundary layer temperature inversions, *Atmos Environ*, 43, 3596-3604, <https://doi.org/10.1016/j.atmosenv.2009.03.049>, 2009.

Wang, S., Xing, J., Chatani, S., Hao, J., Klimont, Z., Cofala, J., and Amann, M.: Verification of anthropogenic emissions of China by satellite and ground observations, *Atmos Environ*, 45, 6347-6358,

<https://doi.org/10.1016/j.atmosenv.2011.08.054>, 2011.

Wang, Y., Yang, K., Pan, Z., Qin, J., Chen, D., Lin, C., Chen, Y., Lazhu, Tang, W., Han, M., Lu, N., and Wu, H.: Evaluation of Precipitable Water Vapor from Four Satellite Products and Four Reanalysis Datasets against GPS Measurements on the Southern Tibetan Plateau, *J Climate*, 30, 5699-5713, 10.1175/JCLI-D-16-0630.1, 2017.

Xu, W. Y., Zhao, C. S., Ran, L., Deng, Z. Z., Liu, P. F., Ma, N., Lin, W. L., Xu, X. B., Yan, P., He, X., Yu, J., Liang, W. D., and Chen, L. L.: Characteristics of pollutants and their correlation to meteorological conditions at a suburban site in the North China Plain, *Atmos. Chem. Phys.*, 11, 4353-4369, 10.5194/acp-11-4353-2011, 2011.

Xue, R., Wang, S., Li, D., Zou, Z., Chan, K. L., Valks, P., Saiz-Lopez, A., and Zhou, B.: Spatio-temporal variations in NO₂ and SO₂ over Shanghai and Chongming Eco-Island measured by Ozone Monitoring Instrument (OMI) during 2008–2017, *Journal of Cleaner Production*, 258, 120563, <https://doi.org/10.1016/j.jclepro.2020.120563>, 2020.

Yin, H., Sun, Y., Liu, C., Zhang, L., Lu, X., Wang, W., Shan, C., Hu, Q., Tian, Y., Zhang, C., Su, W., Zhang, H., Palm, M., Notholt, J., and Liu, J.: FTIR time series of stratospheric NO₂ over Hefei, China, and comparisons with OMI and GEOS-Chem model data, *Opt Express*, 27, A1225-A1240, 10.1364/OE.27.0A1225, 2019.

Yin, H., Sun, Y., Liu, C., Lu, X., Smale, D., Blumenstock, T., Nagahama, T., Wang, W., Tian, Y., Hu, Q., Shan, C., Zhang, H., and Liu, J.: Ground-based FTIR observation of hydrogen chloride (HCl) over Hefei, China, and comparisons with GEOS-Chem model data and other ground-based FTIR stations data, *Opt Express*, 28, 8041-8055, 10.1364/OE.384377, 2020.

Yin, H., Liu, C., Hu, Q., Liu, T., Wang, S., Gao, M., Xu, S., Zhang, C., and Su, W.: Opposite impact of emission reduction during the COVID-19 lockdown period on the surface concentrations of PM_{2.5} and O₃ in Wuhan, China, *Environmental Pollution*, 289, 117899, <https://doi.org/10.1016/j.envpol.2021.117899>, 2021a.

Yin, H., Lu, X., Sun, Y., Li, K., Gao, M., Zheng, B., and Liu, C.: Unprecedented decline in summertime surface ozone over eastern China in 2020 comparably attributable to anthropogenic emission reductions and meteorology, *Environ Res Lett*, 2021b.

Yin, H., Sun, Y., Liu, C., Wang, W., Shan, C., and Zha, L.: Remote Sensing of Atmospheric Hydrogen Fluoride (HF) over Hefei, China with Ground-Based High-Resolution Fourier Transform Infrared (FTIR) Spectrometry, *Remote Sens-Basel*, 13, 791, 2021c.

Yin, H., Sun, Y., Wang, W., Shan, C., Tian, Y., and Liu, C.: Ground-based high-resolution remote sensing of sulphur hexafluoride (SF₆) over Hefei, China: characterization, optical misalignment, influence, and variability, *Opt Express*, 29, 34051-34065, 10.1364/OE.440193, 2021d.

Zhai, S., Jacob, D. J., Wang, X., Shen, L., Li, K., Zhang, Y., Gui, K., Zhao, T., and Liao, H.: Fine particulate matter (PM_{2.5}) trends in China, 2013–2018: separating contributions from anthropogenic emissions and meteorology, *Atmos. Chem. Phys.*, 19, 11031-11041, 10.5194/acp-19-11031-2019, 2019.

Zhang, L., Lee, C. S., Zhang, R., and Chen, L.: Spatial and temporal evaluation of long term trend (2005–2014) of OMI retrieved NO₂ and SO₂ concentrations in Henan Province, China, *Atmos Environ*, 154, 151-166, <https://doi.org/10.1016/j.atmosenv.2016.11.067>, 2017.

Zhang, R., Tie, X., and Bond, D. W.: Impacts of anthropogenic and natural NO_x sources over the U.S. on tropospheric chemistry, *Proceedings of the National Academy of Sciences*, 100, 1505, 10.1073/pnas.252763799, 2003.

Zhang, S., Wang, S., Zhang, R., Guo, Y., Yan, Y., Ding, Z., and Zhou, B.: Investigating the Sources of

Formaldehyde and Corresponding Photochemical Indications at a Suburb Site in Shanghai From MAX-DOAS Measurements, *Journal of Geophysical Research: Atmospheres*, 126, e2020JD033351, <https://doi.org/10.1029/2020JD033351>, 2021.

Zhao, S., Yu, Y., Yin, D., He, J., Liu, N., Qu, J., and Xiao, J.: Annual and diurnal variations of gaseous and particulate pollutants in 31 provincial capital cities based on in situ air quality monitoring data from China National Environmental Monitoring Center, *Environment International*, 86, 92-106, <https://doi.org/10.1016/j.envint.2015.11.003>, 2016.

Zhao, Z., and Wang, Y.: Influence of the West Pacific subtropical high on surface ozone daily variability in summertime over eastern China, *Atmos Environ*, 170, 197-204, <https://doi.org/10.1016/j.atmosenv.2017.09.024>, 2017.

Zheng, B., Tong, D., Li, M., Liu, F., Hong, C., Geng, G., Li, H., Li, X., Peng, L., Qi, J., Yan, L., Zhang, Y., Zhao, H., Zheng, Y., He, K., and Zhang, Q.: Trends in China's anthropogenic emissions since 2010 as the consequence of clean air actions, *Atmos. Chem. Phys.*, 18, 14095-14111, 10.5194/acp-18-14095-2018, 2018a.

Zheng, C., Zhao, C., Li, Y., Wu, X., Zhang, K., Gao, J., Qiao, Q., Ren, Y., Zhang, X., and Chai, F.: Spatial and temporal distribution of NO₂ and SO₂ in Inner Mongolia urban agglomeration obtained from satellite remote sensing and ground observations, *Atmos Environ*, 188, 50-59, <https://doi.org/10.1016/j.atmosenv.2018.06.029>, 2018b.

Zheng, F., Yu, T., Cheng, T., Gu, X., and Guo, H.: Intercomparison of tropospheric nitrogen dioxide retrieved from Ozone Monitoring Instrument over China, *Atmospheric Pollution Research*, 5, 686-695, <https://doi.org/10.5094/APR.2014.078>, 2014.

Zhou, C., Wang, K., and Ma, Q.: Evaluation of Eight Current Reanalyses in Simulating Land Surface Temperature from 1979 to 2003 in China, *J Climate*, 30, 7379-7398, 10.1175/JCLI-D-16-0903.1, 2017.